SCC

How Much CO_2 and the Sun Contribute to Global Warming:

Comparison of Simulated Temperature Trends with Last Century Observations

Correspondence to harde@hsu-hh.de

Vol. 2.2 (2022)
pp. 105-133

Hermann Harde

Helmut-Schmidt-University, Hamburg, Germany

Abstract

The Intergovernmental Panel on Climate Change classifies the human influence on our climate as extremely likely to be the main reason of global warming over the last decades. Particularly anthropogenic emissions of carbon dioxide are made responsible for the observed temperature changes, while any natural forcings are almost completely excluded. However, detailed own calculations with an advanced energy-radiation-balance model indicate that the temperature increase and its variations over the last 140 years can much better be explained by additionally including solar radiative forcing and its amplification by induced cloud cover changes. We present simulations based on different time series of the total solar irradiance and compare them with composed land-ocean-surface temperature measurements of the Northern Hemisphere. From these simulations we follow that CO_2 should not have contributed more than about one third to global warming over the last century, while solar variations over this period can well explain two thirds of the increase.

Keywords: Solar variability; global warming; temperature time series; CO_2 radiative forcing; solar radiative forcing; climate sensitivity; solar sensitivity; thermal feedbacks; solar feedback.

Submitted Dec. 02, 2021. Accepted Feb. 11, 2022. https://doi.org/10.53234/scc202206/10

1. Introduction

The Fifth and Sixth Assessment Report (AR5 and AR6) [1, 2] of the Intergovernmental Panel on Climate Change (IPCC) announced new evidence of an anthropogenic climate change based on many independent scientific analyses from observations of the climate system, paleoclimate archives, theoretical studies of climate processes, and simulations using climate models. In these reports the IPCC classifies the human influence as extremely likely to be the dominant cause of the observed warming since the mid-20th century (e.g., AR5-WG1-SPM-D3), while contributions from natural forcings and internal variability would only likely be in the range of −0.1°C to 0.1°C. Particularly increasing emissions of carbon dioxide (CO_2) over the last century are made responsible for this change, and the Equilibrium Climate Sensitivity (*ECS*) as a measure for the Earth's temperature increase at doubled CO_2 concentration in the atmosphere is specified with an assessed best estimate of 3°C and a *likely* range of 2.5°C to 4°C (high confidence, AR6-WG1-SPM, A.4.4) - acronyms see Annex.

However, explanations of the observed global warming over the last 170 years, in particular anthropogenic contributions to this warming, are still quite contradictorily discussed, and it is surprising:

(i) that the well documented delayed and pure native emissions of CO_2 and methane (CH_4) to sea and air temperature changes (see, e.g., Petit et al. [3]; Monnin et al. [4]; Caillon et al. [5]; Torn & Harte [6]; Humlum et al. [7]; Salby [8]) are not further considered in AR5 or AR6 with their consequences for interpreting actual climate changes (for a detailed con-

sideration of the "hen-or-egg causality" see also Koutsoyiannis & Kundzewicz [9]);

(ii) that any observed increase of CO_2 since the Little Ice Age is allocated only to anthropogenic emissions and assumed to cumulate in the atmosphere over thousands of years, while any temporal and temperature dependent variations of the 25 times larger natural emissions and their uptake are excluded (see, Harde [10, 11]);

(iii) that Radiative Forcings (RF) of greenhouse (GH) gases with their feedbacks are referred, which are mostly valid for clear sky conditions, while the impact of clouds is usually omitted (AR5-WG1- Chap.8.3.1);

(iv) that important effects like convection and evaporation feedback, which can contribute to significant negative feedback (Harde [12, 13]), are not considered;

(v) and that the IPCC denies any noticeable solar influence on the actual climate, although there exists strong evidence of an increasing solar activity over the last century (see, e.g., Hoyt & Schatten [14]; Willson & Mordvinov [15]; Shapiro et al. [16]; Ziskin & Shaviv [17]; Scafetta & Willson [18]; Usoskin et al. [19]; Zhao & Feng [20]; Soon et al. [21]; Connolly et al. [22]).

Despite these deficits and simplifications, the GH-gases are assigned with very high confidence (95%) to be responsible for the actual climate change. Because of the far-reaching consequences for future climate predictions, it is particularly important to scrutinize, how far this assertion can really be confirmed by the observed changes of GH-gas concentrations, the global temperature and the solar activity. Also, the impact of some native effects like thermally and solar induced cloud cover changes, which affect our climate, but which are not always well understood, has carefully to be investigated with its implications on the observed temperature changes.

Therefore, in this contribution we compare composed land and sea surface temperature measurements of the Northern Hemisphere (Soon et al. [21]) with simulations performed by an advanced 2-Layer Climate Model (2LCM) (Harde [12, 13]), which allows to calculate the influence of CO_2 and solar variations on the climate. This model with its main features is briefly presented in Section 2. The different external forcings like the CO_2 radiative forcing and the solar radiative forcing with their specific feedbacks are discussed in Section 3 and can directly be compared with calculations within the Coupled Model Intercomparison Project Phase 5 (CMIP5) and Phase 6 (CMIP6). In Section 4 we present simulations for the temperature trend over the last 140 years, based on the CMIP5 and CMIP6 data, and on the other hand on our own calculations, this for six different Total Solar Irradiance (*TSI*)-time-series, which we oppose to respective measurements. Section 5 gives a summary with future perspectives.

2. Two-Layer-Climate Model

Climate models are the primary tools available for investigating the response of the climate system to various forcings, for making climate predictions on seasonal to decadal time scales and for making projections of future climate over the coming century and beyond (see AR5-Chap.9 [1]).

Over recent years models of different complexity were developed. Atmosphere–Ocean General Circulation Models (AOGCMs) are primarily aiming to understand the dynamics of the physical components of the climate system (atmosphere, ocean, land and sea ice), and to make projections based on future GH-gas and aerosol forcing. These models are extensively used for seasonal to decadal climate predictions, often with a focus on particular regions.

Earth System Models (ESMs) expand on AOGCMs and try to include various biogeochemical cycles such as the carbon-, the sulphur- or ozone-cycle. They are the most comprehensive tools available for simulating the response of the climate to external forcing with biogeochemical feedbacks.

Earth System Models of Intermediate Complexity (EMICs) attempt to include relevant components often in an idealized manner or at lower resolution than the models described above. EMICs are more focussed on certain scientific questions such as understanding climate feedbacks on millennial time scales or exploring sensitivities in which long model integrations are required. This class of models often includes Earth system components not yet included in all ESMs (e.g., ice sheets).

Different to the AOGCMs and ESMs, which with their higher local and temporal resolution have to solve complex coupled nonlinear differential equations - making these calculations extremely time consuming and even unstable - we use a much simpler but not less expressive model, which is based on a global energy and radiation balance and averages over larger local variations. Its primary objective is comparable with EMICs to better understand climate feedbacks and the sensitivity of some impacts, which have not been considered previously in other models. Our direct approach to the model evaluation is to compare model output with observations and to analyse the resulting difference. Figure 1 shows the main features of our model with its relevant parameters.

This model is especially appropriate to calculate the influence of increasing CO_2 concentrations on global warming as well as the impact of solar variations on the climate. It considers the atmosphere and the Earth's surface as two main layers acting as absorbers for short wave (sw) and long wave (lw) radiation and simultaneously working as Planck radiators for lw radiation. In addition, it includes heat transfer between these layers due to convection and evaporation (P_C and P_L), and it considers sw and lw scattering processes at the atmosphere and at clouds. Further it includes all common feedback processes like water vapor, lapse rate, and albedo feedback but additionally takes into account temperature dependent sensible and latent heat fluxes as well as temperature induced and solar induced cloud cover feedback.

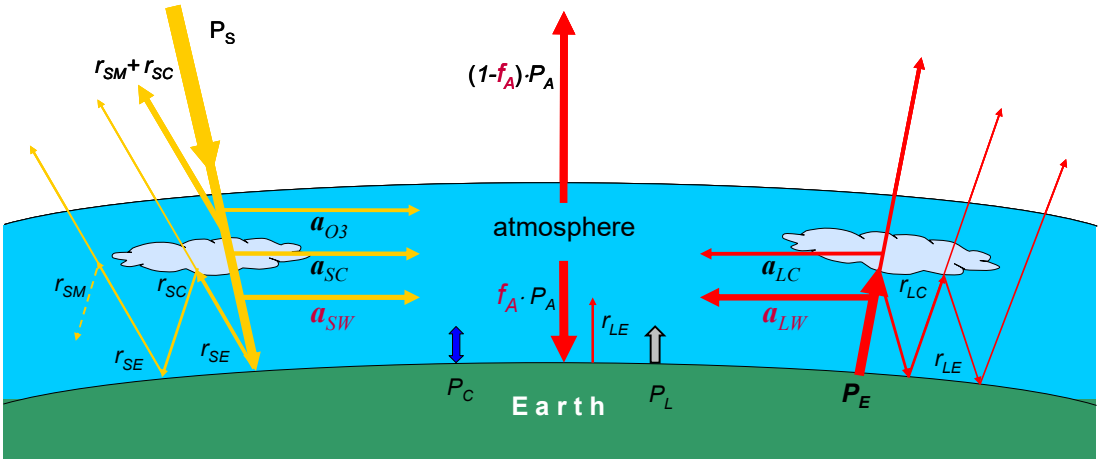

P – power; r – reflectivity (scattering); a – absorptivity; f_A – back-radiated fraction

Figure 1: Two-layer climate model for the Earth-atmosphere system with the main parameters.

At equilibrium the Earth's surface and atmosphere release as much power as they suck up from the Sun and the neighbouring layer. This gives a coupled balance equation system, which can be solved for the radiated power P_E of the surface and the emitted power P_A of the atmosphere. With Stefan-Boltzmann's law the global mean temperatures at the surface and for the atmosphere are derived.

Primarily this 2LCM was developed to assess the Equilibrium Climate Sensitivity *ECS* and also the Equilibrium Solar Sensitivity *ESS* (temperature change at 1‰ variation of the Total Solar Irradiance *TSI*), i.e., it uses steady-state conditions for the energy and radiation balance to derive from this the respective Earth and atmospheric temperatures T_E and T_A at a given CO_2 concentration and *TSI*. But such calculation can also be applied to track the smaller temperature variations caused by the year-to-year CO_2 and *TSI* changes. The faster adjustments to the RF like

tropospheric and stratospheric temperature adjustments already achieve equilibrium within a few months, only the surface temperature is adapting over much longer periods. But with CO_2 concentration changes of about 130 ppm over 170 years, corresponding to an average increase of 0.8 ppm/yr, also the slower thermal feedbacks are all the time close to equilibrium conditions, which compared to a transient response only slightly shift the absolute temperature level by not more than one or two tenth of a degree. At the same time this defines an upper limit of these impacts without affecting their relative contributions to global warming. In addition, for comparison with the observed temperature series, which are expected to suffer from a larger delay to an internal or external forcing, the calculated temperatures in any way have to be considered as moving average over 15 to 20 years, thus, further reducing any differences between the transient response and the equilibrium climate calculations.

Different to other climate models, where the influence of GH-gases is expressed by the radiative forcing F_{RG} in the tropopause, in this model the key parameters controlling the fluxes are the sw- and lw-absorptivities a_{SW} and a_{LW} of the GH-gases as well as the back-radiated fraction f_A of the atmosphere (see Fig. 1.) These parameters are changing with the atmospheric composition of the gases, their partial and total pressure as well as with their temperature. This requires detailed Line-By-Line sw absorption and lw Radiation Transfer (LBL-RT) calculations for the up- and down-welling fluxes in the atmosphere (for details see Harde [12, 13, 23, 24]), this for different CO_2 concentrations (in this case 14 concentrations from 0 - 770 ppm), for three climate zones with different ground temperatures and humidity, and for different cloud covers. Such calculations include up to 900,000 lines for the most important GH-gases water vapor (WV), carbon dioxide, methane, and ozone and are based on the HITRAN database [25].

Since the partial pressure of the GH-gases and the atmospheric pressure are changing with temperature and altitude, the atmosphere is segmented into up to 228 sub-layers from ground to 86 km height. The layer thickness up to the tropopause is 100 m and is increasing over the stratosphere. For each slice the individual spectral absorptivities and re-emission are calculated, summed up over the propagation path and are integrated over the spectral distribution to obtain the respective key parameters for the different CO_2 concentrations, for different ground temperatures (with changing WV concentrations), and for different cloud covers. With these parameters integrated in the climate model, the Earth's surface temperature T_E and the lower tropospheric temperature T_A (in about 800m altitude) are simulated as a function of the CO_2 concentration and the solar anomaly. For comparison with other models from these data we also derive the CO_2 radiative forcing F_{CO2}.

Pressure and temperature changes with altitude are based on the US Standard Atmosphere Model (for details see Harde [12], Subsec. 2.1.2). Some other parameters (cloud and sw ozone absorptivities, scattering coefficients at clouds and the atmosphere, as well as the sw and lw Earth's reflectivities) are adapted in such a way that all radiation and heat fluxes almost exactly reproduce the widely accepted radiation and energy budget scheme of Trenberth, Fassulo and Kiehl (TFK-scheme) [26], which essentially relies on data from satellite measurements within the ERBE and CERES program [27–31]. This adaptation yields a calibration of the model to the observed up- and downwelling fluxes under standard conditions in the atmosphere and for constant heat fluxes between the surface and atmosphere.

To reproduce also the measured temperature variations with the observed cloud cover changes over the 80s and 90s, we relate to the temperature anomaly data of the Hadley Centre and Climate Research Unit (HadCRUT3) as a function of the monthly global cloud cover data of the International Satellite Cloud Climatology Project (ISCCP) [32] yielding a response of −0.065°C/% of cloud cover changes (see also O. Humlum [33]).

All relevant parameters are listed in Harde [13], Table 6. Together with an assumed TSI = 1365.2 W/m^2, a mean cloud cover C_C = 66% and a CO_2 concentration of 380 ppm they determine a reference temperature T_R = 16°C of the Earth's surface (see TFK-scheme [26]). Since over the period from 1850 to present the CO_2 concentration increased from 280 to actually 410

ppm, and most of the *TSI* time series investigated in this contribution are varying around a mean *TSI* of 1360 W/m^2, it is preferential to avoid larger deviations from the reference, particularly for feedbacks with a larger non-linear response. Therefore, we use here as references for our simulations the lower *TSI* of S_R = 1360 W/m^2 and a lower CO_2 concentration of C_R = 350 ppm, which together with the other parameters now define a reference temperature of T_R = 15.5°C. These references together tie up a working point, around which smaller deviations in the CO_2 concentration and the solar anomaly are considered.

3. External Forcings and their Feedbacks

For our actual studies, which aim towards distinction of anthropogenic and natural contributions to global warming, it is important to clearly assign the different drivers and forcings with their respective feedbacks. This is the subject of this section. The strength of drivers is quantified as radiative forcing RF in units of W/m^2 and represents the change in energy flux caused by a driver. It is calculated at the tropopause or at the top of the atmosphere.

Independent of the model's complexity, almost all known models are based on the simple relation that the ground temperature changes ΔT_E^i are scaling proportional to the changes of an external forcing ΔF_i :

$$\Delta T_E^i = \lambda_i \cdot \Delta F_i , \tag{1}$$

where λ_i is a sensitivity parameter representing the response of the Earth-Atmosphere-System (EASy) to the forcing. This equation holds for transient as well as for equilibrium conditions. The IPCC assigns almost all global warming to the emitted GH-gases and in particular to the impact of CO_2. Therefore, here we only consider the increase of the CO_2 concentration over the Industrial Era from 280 ppm to 410 ppm, while any contributions due to CH_4 or N_2O variations can well be neglected.

3.1 CO_2 Radiative Forcing

With (1) then we can write for the temperature increase due to CO_2 radiative forcing ΔF_{CO2} (units: W/m^2):

$$\Delta T_E^{CO2} = \lambda_P \cdot \Delta F_{CO2} = -\frac{1}{\alpha_P} \Delta F_{CO2} , \tag{2}$$

with λ_P as the Planck sensitivity or climate sensitivity parameter and α_P as the Planck response or Planck feedback, which represents the additional thermal or lw emission to space arising from vertically uniform warming of the surface and the atmosphere (AR6-WG1-Chap.7.4.2.1). It plays a fundamental stabilizing role in Earth's climate and has a strongly negative value: a warmer planet radiates more energy to space.

A calculation of the Earth's temperature T_E with the 2LCM as a function of the CO_2 concentration is displayed in Fig. 2 (Red Diamonds, for further details see also Harde [13], Subsec. 4.2).

In good agreement with the literature (e.g., Myhre et al. 1998 [34]) for higher concentrations our LBL-RT calculations reveal an almost logarithmic increase (Green Triangles) of the CO_2 forcing with rising CO_2 concentration C_{CO2} relative to the reference concentration C_R of 350 ppm:

$$\Delta T_E^{CO2} = \lambda_P \cdot \Delta F_{2xCO2} \frac{\ln(C_{CO2}/C_R)}{\ln 2} = ECS_B \frac{\ln(C_{CO2}/C_R)}{\ln 2} . \tag{3}$$

For doubling the concentration from 350 to 700 ppm, at a mean cloud cover of 66% we find a forcing of ΔF_{2xCO2} = 3.69 W/m^2 ([13], Table 3). However, due to some deviations from a pure logarithmic progression, for smaller concentrations from 280 to 560 ppm this reduces to ΔF_{2xCO2} = 3.32 W/m^2. Since forcing and *ECS* are mostly considered for a doubling of CO_2 from pre-

industrial times with 280 ppm to 560 ppm, here we also relate to these changes - different to [13].

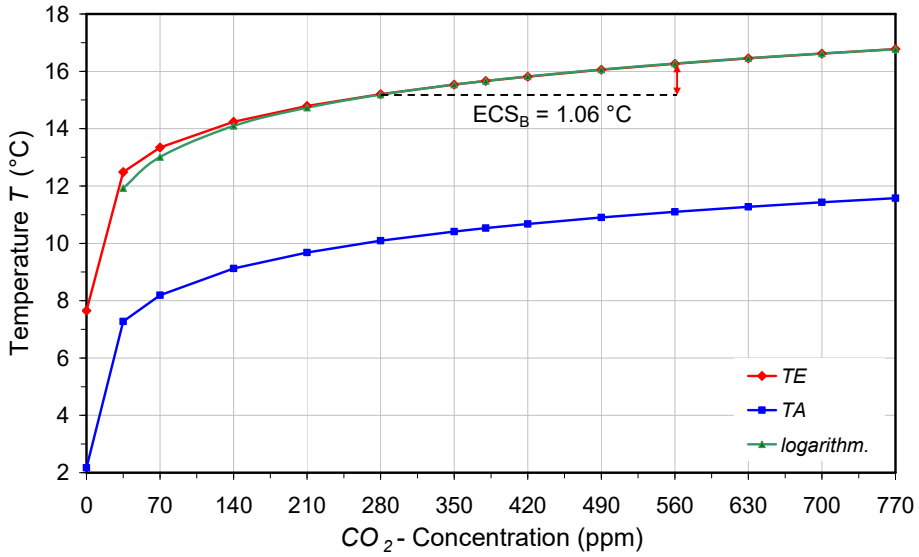

Figure 2: Calculated Earth temperature T_E (Red Diamonds) and atmospheric temperature T_A (Blue Squares) as a function of increasing CO_2 concentration at mean cloud cover without feedbacks. The Earth temperature can well be represented by a logarithmic graph (Green Triangles) with a basic equilibrium climate sensitivity ECS_B = 1.06°C.

For the 2LCM with its key parameters a_{SW}, a_{LW} and f_A we then calculate a basic *ECS* (without feedbacks) of ECS_B = 1.06°C (see Fig. 2, Red Diamonds), and with $\lambda_P = ECS_B/\Delta F_{2xCO2}$ together with the above forcing a Planck sensitivity λ_P = 0.319 °C/(W/m^2).

The atmospheric temperature T_A (Blue Squares) reflects the temperature of the lower troposphere in an altitude of about 800 m as a function of the CO_2 concentration (for details see [12], Subsec. 4.4).

We note that the climate sensitivity, which we derive from a radiation and energy balance at the surface and TOA, also includes atmospheric sw absorptivity changes, while the forcing $\Delta F_{2\times CO2}$ = 3.32 W/m^2 only represents the instantaneous lw RF at TOA (without stratospheric adjustment). With AR5 the IPCC introduced the concept of an effective RF, which includes short-time adjustments. However, for a simulation with the 2LCM another RF only changes the Planck sensitivity, not the basic equilibrium climate sensitivity as the relevant quantity for our further investigations.

This basic climate sensitivity with $ECS_B = \lambda_P * \Delta F_{2xCO2}$ = 1.06°C exactly reproduces the value used in the CMIP5 AOGCMs (see AR5-WG1-Tab.9.5), only the forcing of CMIP5 with ΔF_{2xCO2} = 3.39 W/m^2 is 2% larger, and thus the Planck sensitivity with $\lambda_P = -1/\alpha_P$ = 0.313°C/W*m^2 accordingly smaller. A second approach listed in AR5-WG1-Tab.9.5 uses an RF of 3.71 W/m^2 with the same Planck sensitivity and therefore calculates with an ECS_B = 1.16°C. The CMIP6 ESMs actually emanate from values for λ_P = 0.311°C/W*m^2 and for ΔF_{2xCO2} = 3.93 W/m^2 with an ECS_B = 1.22°C (AR6-WG1-Chap.7.4).

3.1.1 Thermal Feedbacks

However, by far the largest inconsistencies between different climate models result from feedback processes. Their combined effect is to amplify the base climate response (Planck response), and they are mainly responsible that the *ECS* as one of the most important but also most controversially discussed measures in climate science diverges by more than a factor of 20 from about 0.4 up to more than 8°C.

Certainly one reason of these large discrepancies is the complexity of some effects, from which their interrelated actions and their mutual interference are often not really known. Other reasons are the wrong or undifferentiated assignment of a feedback to a specific climate driver, and also the simple neglect of effects.

Feedback effects are generally included in (1) or (2) as additional terms, which to first order are assumed to respond linearly and independently to the temperature changes ΔT_E. Eq. (2) then extends to:

$$\Delta T_E^{CO2} = \lambda_P \cdot (\Delta F_{CO2} + \sum_k f_k \cdot \Delta T_E^{CO2}), \tag{4a}$$

or after transposition

$$\Delta T_E^{CO2} = \frac{1}{1-\lambda_P \cdot \sum f_k} \cdot \lambda_P \cdot \Delta F_{CO2} = \lambda_P \cdot A_{FT} \cdot \Delta F_{CO2}, \tag{4b}$$

where the f_k designate different feedbacks (units: W/m²/°C) and $A_{FT} = (1-\lambda_P \cdot \Sigma f_k)^{-1} = \alpha_P/(\alpha_P+\Sigma f_k)$ is the thermal feedback amplification or attenuation factor of the radiative forcing. While in AR6 feedbacks are now abbreviated as α_k, here we further use f_k.

CMIP5 explicitly considers 4 feedbacks (AR5-WG1-Tab.9.5), which are listed in Table 1, column 2 as the mean of 30 AOGCMs. For the sake of clarity, only the values for the lower RF are listed in Table 1. CMIP6 additionally discusses biogeochemical and biogeophysical feedbacks (AR6-WG1-Chap.7.4), but does not closer specify their size. The average of 35 models with an even larger spread than CMIP5, is listed in column 3.

Table 1: Thermal feedbacks for CO_2 radiative forcing

	CMIP5			**CMIP6**			**2LCM**		
λ_P (°C/W·m²)	0.313			0.311			0.319		
ΔF_{2xCO2} (W/m²)	3.39			3.93			3.32		
ECS_B (°C)	1.06			1.22			1.06		
feedbacks	f_k W/m²/°C	A_k	ΔT_k °C	f_k W/m²/°C	A_k	ΔT_k °C	f_k W/m²/°C	A_k	ΔT_k °C
water vapor f_{WV}	1.6	2.0	1.06	1.77	2.22	1.5	0.38	1.14	0.14
lapse rate f_{LR}	–0.6	0.84	–0.17	–0.50	0.87	–0.16	–0.6	0.84	–0.17
surf. albedo f_{SA}	0.3	1.10	0.11	0.35	1.12	0.15	0.3	1.11	0.11
clouds therm f_{TC}	0.3	1.10	0.11	0.49	1.18	0.22	0.3	1.11	0.11
convection f_{CO}							–0.02	0.99	–0.01
evaporation f_{EV}							–2.51	0.55	–0.47
total feedbacks by CO_2	f_{TG} W/m²/°C	A_{FT}	***ECS*** °C	f_{TG} W/m²/°C	A_{FT}	***ECS*** °C	f_{TG} W/m²/°C	A_{FT}	***ECS*** °C
	2.14	3.01	**3.2**	2.18	3.10	**3.78**	-1.77	0.64	**0.68**

Water-Vapor-Feedback: While the lapse-rate, the surface albedo and the thermally induced cloud changes only moderately affect the ground temperature changes, the IPCC assumes as the dominant impact on global warming the water vapor feedback (AR6-WG1-Chap.7.4.2.2). CMIP5 uses a feedback of f_{WV} = 1.6 W/m²/°C, yielding an amplification of the basic ECS_B of

A_{WV} = 2, CMIP6 even emanates from f_{WV} = 1.77 W/m²/°C with an amplification of A_{WV} = 2.22 (for an assessment of feedbacks, see also AR6-WG1-Tab.7.10 and Fig.7.10).

Our own investigations, however, show a significantly smaller influence of WV. From LBL-RT calculations for three different climate zones and thus different temperatures and humidity we derive a water vapor feedback of f_{WV} = 0.38 W/m²/°C with an amplification at mean cloud cover of only A_{WV} = 1.14 or +14% (for details see, Harde [13], subsection 4.3.1). The reasons for this discrepancy are fourfold:

(i) So, our calculations also consider the sw absorptivity, which causes negative feedback. Apparently, this contribution is not considered and specified in AR5. Whereas the lw outgoing radiation is more efficiently blocked and thus contributes to positive feedback, the sw radiation is also more strongly absorbed with increasing WV in the atmosphere and less of it reaches the surface, which contributes to slightly negative feedback.

(ii) Further, the IPCC neglects a declining absorption cross-section of GH-gases with increasing temperature over the troposphere (see Harde [24]).

(iii) The main differences, however, relate to cloud and saturation effects. In AR5-WG1-Chap.8.3.1 we can read that "*most intercomparison studies of the RF of GH-gases are for clear sky and aerosol-free conditions, while the introduction of clouds would greatly complicate the targets of research and are usually omitted in the intercomparison exercises of GCM radiation codes and LBL codes*".

Therefore, obviously also for an assessment of the WV feedback cloud effects were neglected. Our studies show that calculations for clear sky give a feedback of f_{WV} = 1.04 W/m²/°C with an amplification A_{WV} = 1.54, which for its own already contributes to a 4x larger temperature increase of 54% compared to mean cloudiness conditions with only 14%. Since at clear sky also the ECS_B with 1.68°C is much larger than at 66% cloud cover with 1.06°C, this would result in an increase due to WV-feedback of ΔT_E = 1.54x1.68°C = 2.59°C, while at mean cloudiness this does not contribute more than ΔT_E = 1.14x1.06°C = 1.2°C.

(iv) Finally, most of the AOGCMs emanate from a mean WV concentration of 7,750 ppm, in agreement with the US Standard Atmosphere 1976, representing mid-latitude but not global mean conditions. In our calculations we use a global mean WV concentration (at standard conditions) of 14,615 ppm, which was derived from GPS measurements (Vey [35]) of the water content in different climate zones (see Harde [12], Fig. 1).

Similar to CO_2, also the water lines are already strongly saturating over wider spectral regions. Therefore, with increasing vapor concentration only the far wings of these lines and weak absorption bands can further contribute to an additional absorption, which roughly logarithmically increases with the vapor concentration. Despite an exponential increase of the vapor concentration with rising temperature, due to the Clausius-Clapeyron relation together this only results in a linear increase of the absorptivities. For the lw absorptivity, e.g., this increase with temperature is only one third under global mean conditions compared to US Standard Atmosphere conditions.

Altogether, consideration of the sw and lw effects with temperature, the strong impact of clouds and the larger saturation at higher water vapor level leads to a significantly lower response to temperature changes than assumed in most AOGCMs and ESMs. So, our analysis of the WV feedback only contributes to an increase of the basic climate sensitivity of 14%, while the IPCC follows from a gain of 120%, which is more than 8 times larger.

Lapse-Rate and Surface Albedo Feedback: When the vertical temperature profile changes, also the back-radiation varies with temperature and concentration changes of the GH gases. As a direct consequence also the radiation balance is modified and known as lapse rate feedback.

Both theory and climate models indicate that global warming will reduce the rate of temperature decrease with altitude, producing a negative lapse rate feedback, considered in CMIP5 with f_{LR} = −0.6 W/m²/°C (AR5-WG1-Tab.9.5), in CMIP6 with −0.5 W/m²/°C (AR6-WG1-Chap.7.4.2). In our accounting scheme this is expressed as a temperature dependent back-radiated fraction df_A/dT_E = −0.0875%/°C with an attenuation of A_{LR} = 0.84.

The surface albedo influence is estimated as a positive feedback, in CMIP5 with f_{SA} = 0.3 ± 0.1 W/m²/°C, in CMIP6 with f_{SA} = 0.35 ± 0.1 W/m²/°C. In our simulations we introduce this albedo feedback as a temperature dependent change of the Earth's reflectivity with dr_{SE}/dT_E = −0.158 %/°C, which at mean overcast contributes to an increase of the climate sensitivity of 11%.

For the lapse-rate and the surface albedo these are the same feedbacks as specified in AR5-WG1-Tab.9.5.

Cloud-Feedback: *"Clouds respond to climate forcing mechanisms in multiple ways, and differences in cloud feedbacks constitute by far the primary source of spread of both equilibrium and transient climate responses simulated by climate models"* (Dufresne & Bony [36]).

So, quite contradictory observations are reported, where on the one side regional meteorological conditions over the Pacific are described, providing modelling evidence for a positive low level cloud feedback in this region on decadal time scales (Clement et al. [37]), and on the other side, particularly in the tropics, the opposite trend is observed that with increasing temperature and thus rising humidity also the cloud formation is increasing, which then contributes to negative feedback (Lindzen et al. [38]; Laken & Pallé [39]; Cho et al. [40]; Caldwell et al. [41]).

The IPCC exclusively considers a Thermally Induced Cloud (*TIC*)-feedback f_{TC} and lists in AR6-WG1-Chap7.4.2.4.3 a best estimate of the net cloud feedback of f_{TC} = 0.42 W/m²/°C with a *very likely* range of -0.1 to 0.94 W/m²/°C, which is less than the value published in AR5 with f_{TC} = 0.6 (−0.2 to +2.0) W/m²/°C (see AR5-WG1-Chap.7). On the other hand, CMIP5 models were assuming a model mean half of f_{TC} = 0.3 ±0.7 W/m²/°C (AR5-WG1-Tab.9.5), while CMIP6 now uses a value of f_{TC} = 0.49 ±0.6 W/m²/°C. This new and higher cloud feedback together with the water vapor feedback and also the higher assumed RF of ΔF_{2xCO2} = 3.93 W/m² determine the main difference between CMIP5 and CMIP6. At the same time it flattens the discrepancies between the different specified values.

But even the largest value by far cannot explain the observed cloud cover changes over the 80s and 90s within the ISCCP program. This would require an $f_{TC} \geq 2$ W/m²/°C and together with the other feedbacks used in CMIP5/6 then lead to an unrealistically high *ECS* of more than 15°C. Also, with the smaller WV-feedback as derived from our calculations and assuming a cloud feedback of 2 W/m²/°C would give an *ECS* of 2.8°C and contribute to 1.7°C to global warming over the last century, much more than observed.

All this is a strong indication that apparently still another mechanism is responsible for cloud changes which are in agreement with the ISCCP observations. This has to be discussed in the next subsection. But to account also for a thermal impact on cloud changes, in our further simulations we include a CO_2 and thus thermally induced feedback as used in CMIP5 with f_{TC} = 0.3 W/m²/°C.

Convection Feedback: Additionally, to these standard feedbacks we see from our calculations that the air temperature is less sensitively responding to CO_2 concentration changes than the Earth temperature (see Fig. 2). Therefore, the temperature difference in the convection zone is further increasing with ascending CO_2 concentration. As a consequence, also the sensible heat flux of about 17 W/m² is growing with the concentration, which altogether results in negative feedback. A more detailed consideration shows that this feedback is larger for clear sky and reduces at mean cloud cover to f_{CO} = −0.02 W/m²/°C with a damping of 1% (differences to [12], subsection 4.4 and 5.4.4, and [13], subsection 4.3.4 result from considering here a doubling of CO_2 from 280 to 560 ppm).

Evaporation Feedback: Similar to convection also evaporation of water and sublimation of ice contribute to cooling of the surface. Since an increasing Earth temperature further forces these processes, they also result in negative feedback, which we call evaporation feedback.

Although in more general terms this is also one part of convection, we further distinguish convection and evaporation feedbacks to assign them to sensible and latent heat contributions. According to Kirchhoff's equation changes in latent heat are directly proportional to temperature changes with a proportionality factor, given by the difference of the specific heats in the two phases.

From this we derive for a latent heat flux of 80 W/m^2 an evaporation feedback at clear sky of f_{EV} = –2.0 W/m^2/°C with an attenuation factor A_{EV} = 0.59, and at mean cloud cover this results in an even larger negative feedback of f_{EV} = –2.51 W/m^2/°C, yielding an attenuation factor of A_{EV} = 0.55. So, latent heat can contribute to significant negative feedback and work as a strong stabilizer for the climate system. All the more, it is surprising that apparently this feedback is not considered in CMIP5/6 and also not mentioned in AR5 or AR6.

3.1.2 Total Feedback and ECS

CMIP5 specifies a model mean *ECS* of 3.2°C, however, obviously this is in clear contradiction to the mainstream feedback theory. With a Planck sensitivity of λ_P = 0.313 °C/W·m^2 as negative reciprocal of the model mean Planck feedback α_P = –3.2 W/m^2/°C (see AR5-Tab.9.5) and for a total feedback of 1.6 W/m^2/°C (sum of the four feedbacks in column 2, Table 1) the respective amplification should be A_{FT} = 2. Thus, from (4b) with an ECS_B = 1.06°C we only expect an *ECS* = 2.12°C or with the other CMIP5-approach (ECS_B = 1.16°C) an *ECS* = 2.32°C.

For the CMIP6 ESMs the discrepancy to the mainstream theory is less obvious but still noticeable. With a minimally smaller Planck sensitivity of λ_P = 0.311 °C/W·m^2 and a total feedback of 2.11 W/m^2/°C now the respective amplification should be A_{FT} = 2.91; and with an ECS_B = 1.22°C we deduce an *ECS* = 3.55°C, while CMIP6 lists a model mean of 3.78°C (AR6-WG1-Table7.SM.5).

Indeed, it is well known that generally different feedback processes do not act linearly and independently of each other, so that for stronger impacts a larger nonlinear response is expected. For reliable calculations, therefore, it is strongly recommended to consider the different effects simultaneously, but in quite small steps for the energy budget and to repeat this procedure till self-consistency of the balance equation system for the radiated power of the surface P_E and of the atmosphere P_A is achieved.

So, when applying this method and inserting the feedbacks as displayed in Table 1, for CMIP5 only a slightly increasing total feedback and amplification with f_{TG} = 1.63 W/m^2/°C and A_{FT} = 2.03 can be found, while for CMIP6 with f_{TG} = 2.18 W/m^2/°C and A_{FT} = 3.10 we derive values, which now exactly reproduce the specified *ECS* of CMIP6 with 3.78°C.

For the 2LCM with a total negative feedback we observe the opposite behavior. While the direct sum of feedbacks in Table 1, column 4, is –2.16 W/m^2/°C with an amplification A_{FT} = 0.59, the self-consistency calculation gives f_{TG} = –1.77 W/m^2/°C and an A_{FT} = 0.64 with an *ECS* = 0.68°C.

So, to attain for CMIP5 an *ECS* = 3.2°C, a significantly higher total feedback of f_{TG} = 2.14 W/m^2/°C is required yielding an amplification of A_{FT} = 3.01. For our later simulations this is achieved by increasing the respective cloud feedback from f_{TC} = 0.3 to 0.74 W/m^2/°C.

However, the main discrepancies of CMIP5/6 to our approach result from the much larger WV feedback and neglect of negative evaporation feedback (see Table 1, right). At mean cloud cover we get a very moderate *ECS* of only 0.68°C. Thus, the CO_2 contribution to global warming is found to be 5.6x smaller than derived from CMIP6.

3. 2 Solar Radiative Forcing

As pure native contribution to global warming we consider here only variations caused by the solar anomaly. In analogy to (2) we can write for the temperature increase due to solar radiative forcing changes ΔF_{Sun}:

$$\Delta T_E^{Sun} = \lambda_{Sun} \cdot \Delta F_{Sun}\,, \tag{5}$$

with λ_{Sun} = 0.065 W^{-1}m^2 °C as the solar sensitivity parameter, which now reflects the temperature response of the 2LCM to the incident solar intensity at mean cloud cover. For $\Delta F_{Sun} = \Delta TSI$ = 0.1% of the reference intensity S_R = 1360 W/m^2 this defines the basic equilibrium solar sensitivity with ESS_B = 0.088°C.

3.2.1 Solar Induced Thermal Feedback

The solar induced temperature changes underlie the same thermal feedbacks as the CO_2 radiative forcing and can be included as an additional term in (5) similar to (4a) with:

$$\Delta T_E^{Sun} = \lambda_{Sun} \cdot \Delta F_{Sun} + \lambda_P \cdot \sum_k f_k \cdot \Delta T_E^{Sun}\,, \tag{6a}$$

which now is proportional to ΔT_E^{Sun}, and after transposing (6a) this gives

$$\Delta T_E^{Sun} = \frac{1}{1-\lambda_P \cdot \sum f_k}\,\lambda_{Sun} \cdot \Delta F_{Sun} = \lambda_{Sun} \cdot A_{FT} \cdot \Delta F_{Sun}\,. \tag{6b}$$

But different to (4b) now we have to differentiate on the one hand between the temperature response due to the solar influence described by λ_{Sun}, and on the other hand the response of the feedbacks, which due to their definition relate to the Planck sensitivity λ_P. We call this a Solar Induced Thermal (*SIT*)-feedback f_{ST}. With a total feedback amplification factor $A_{FT} = ECS/ECS_B$ = 3.10 under CMIP6 conditions the solar sensitivity becomes $ESS = A_{FT} \cdot ESS_B$ = 0.27°C, while in our case it reduces to 0.06°C and is almost negligible. But nature is somewhat more complicated and presents us always new challenging puzzles.

3.2.2 Solar Induced Cloud Feedback

Various investigations of the solar anomaly over the last century indicate a much larger response of the global temperature on solar radiation than this can be explained only by thermal feedbacks (see, e.g., Ziskin & Shaviv [17]; Vahrenholt & Lüning [42]; Harde [12,13]; Soon et al. [21]; Connolly et al. [22]). Since observations also show that the cloud cover varies over the solar cycles, there exists strong evidence that the solar activity directly acts back on the cloud formation. Actual publications indicate that with an increasing solar activity and, therefore, an increasing solar magnetic field the cosmic flux, which hits the atmosphere, is reduced and causes direct feedback on the cloud cover C_C (for a comprehensive summary see Svensmark [43]). So, it is expected that the generation rate of aerosols as condensation seeds for the formation of water droplets in the lower atmosphere is directly influenced by the cosmic radiation flux (Svensmark-effect), which therewith also controls the cloud cover.

A reduced cloud formation at an increased solar activity then reinforces the initial *TSI* induced temperature increase, and it can be included in the 2LCM as a feedback term, which now is controlled by variations of the *TSI* and initiates reciprocal changes in the cloud cover C_C (see Harde [13], Eq.(21)):

$$C_C(TSI) = \begin{cases} C_{C,\min} + (C_{CR} - C_{C,\min}) \cdot e^{-s_f (TSI - S_R)/S_R} & for\ TSI \geq S_R \\ C_{CR} \quad + (C_{CR} - C_{C,\min}) \cdot (1 - e^{s_f (TSI - S_R)/S_R}) & for\ TSI < S_R \end{cases}, \tag{7}$$

with S_R as the reference solar constant and s_f as a solar induced cloud cover parameter.

Since even at very high *TSI* values clouds would not completely disappear, we suppose a rest cloudiness of $C_{C,min}$ = *20 %* and an exponential approach to this lower limit. For *TSI* values smaller than the reference solar constant S_R we use for reasons of uniqueness the same functional relation.

In our simulations we do not differentiate between low- and high-level cloud contributions but use a more general description, how such feedback can be derived and quantified from observations within the ISCCP program. So, the cloud cover variation from 1983 to 2000 of –4% at an observed *TSI* increase of Δ*TSI* = 0.1% (Willson & Mordvinov [15]) can be reproduced by a cloud cover parameter $s_f = 90$. A smaller supposed increase of only Δ*TSI* = 0.05%, as assumed in some other publications (Fröhlich & Lean [44]), raises s_f to ≈ 180 and thus increases the respective Solar Induced Cloud (*SIC*)-feedback f_{SC}.

With this additional feedback integrated in the 2LCM, analogous to (4a) and (6a), but now with a feedback term which relates to λ_{Sun}, we can write (for the moment still without thermal feedback):

$$\begin{aligned} \Delta T_E^{Sun} &= \lambda_{Sun} \cdot \left(\Delta TSI + f_{SC} \cdot \Delta T_E^{Sun}\right) \;\Rightarrow \\ \Delta T_E^{Sun} &= \frac{1}{1-\lambda_{Sun} \cdot f_{SC}} \lambda_{Sun} \cdot \Delta TSI = \lambda_{Sun} \cdot A_{SC} \cdot \Delta TSI \end{aligned} \quad . \tag{8a}$$

For a cloud cover parameter of $s_f = 90$ the respective *SIC*-feedback becomes f_{SC} = 11.0 W/m²/°C and the *SIC*-amplification factor A_{SC} = 3.5. This feedback includes all sw and lw effects, which are responding to cloud cover changes in our model. Under these conditions the basic solar sensitivity of *0.088°C* rises to *ESS = 0.31°C.* For s_f = 180 the feedback inclines nonlinear to f_{SC} = 12.7 W/m²/°C, the amplification becomes A_{SC} = 5.7 and the solar sensitivity *ESS* = 0.51°C .

An equivalent formulation for *SIC*-feedback is to express this as amplification of the *TSI* changes with a feedback factor $f'_{SC} = \lambda_{Sun} \cdot f_{SC}$ (for $s_f = 90$, e.g.: f'_{SC} = 0.72) and the same amplification A_{SC}:

$$\begin{aligned} \Delta F_{Sun} &= \Delta TSI + f'_{SC} \cdot \Delta F_{Sun} \;\Rightarrow \\ \Delta F_{Sun} &= \frac{1}{1-f'_{SC}} \Delta TSI = A_{SC} \cdot \Delta TSI \end{aligned} \quad . \tag{8b}$$

3.2.3 Combined Solar Induced Thermal and Cloud Feedback

Inserting (8b) into (6b) gives the total temperature change caused by solar radiative forcing, now including *SIT*-and *SIC*-feedbacks:

$$\begin{aligned} \Delta T_E^{Sun} &= \frac{1}{1-\lambda_P \cdot \sum f_k} \lambda_{Sun} \cdot \left(\frac{1}{1-\lambda_{Sun} \cdot f_{SC}} \Delta TSI\right). \\ &= \lambda_{Sun} \cdot A_{FT} \cdot A_{SC} \cdot \Delta TSI \end{aligned} \tag{9}$$

For a solar variability of Δ*TSI* = 0.1%, a *SIC*-amplification A_{SC} = 3.5 and a thermal feedback amplification of A_{FT} = 0.64 for the 2LCM (Table 1, right column) we calculate an equilibrium solar sensitivity of *ESS* = 0.20°C, while with the CMIP6 data this would rise up to 0.96°C, more than the observed temperature increase over the last century.

3. 3 Total Temperature Change

The total temperature change as the sum of (4b) and (9) then gives:

$$\begin{aligned} \Delta T_E &= \frac{\lambda_P}{1-\lambda_P \cdot \sum f_k} \cdot \left(\Delta F_{CO2} + \frac{\lambda_{Sun}/\lambda_P}{1-\lambda_{Sun} \cdot f_{SC}} \Delta TSI\right), \\ &= \lambda_P \cdot A_{FT} \cdot \left(\Delta F_{CO2} + \kappa \cdot A_{SC} \cdot \Delta TSI\right) \end{aligned} \tag{10}$$

with $\kappa = \lambda_{Sun}/\lambda_P$ as ratio of the solar to Planck sensitivity.

Fig. 3 displays the respective block diagram for the CO_2 and solar radiative forcings with their feedbacks and represents the principal scheme, how the Earth's temperature is affected by these external forcings. We note that this is only a first order (linear) approach for the two forcings with their feedbacks to better address the different processes. In any way, the further simulations of the temperature trend as a function of the CO_2 concentration and solar variability over time have to be performed by solving the radiation and energy balance system in smaller steps for all forcings and feedbacks simultaneously, till self-consistency of the radiated power of the surface P_E and of the atmosphere P_A is obtained. This accounts for all kinds of nonlinearities and inter-relations of the different contributions.

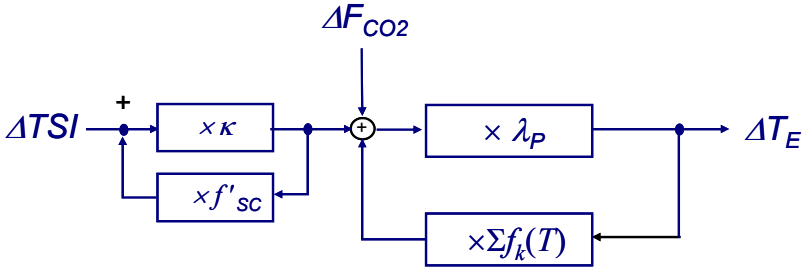

Figure 3: Schematic block diagram of the forcings with their feedbacks.

Table 2 contains a compilation of the climate and solar sensitivities with the respective feedbacks.

Table 2: Equilibrium climate and solar sensitivity for the CMIP5/6 models and the 2LCM.

	CMIP5			**CMIP6**			**2LCM**		
***ECS*$_B$** (°C)	1.06			1.22			1.06		
CO_2 feedback	f_{TG} W/m²/°C	A_{FT}	***ECS*** °C	f_{TG} W/m²/°C	A_{FT}	***ECS*** °C	f_{TG} W/m²/°C	A_{FT}	***ECS*** °C
	2.14	3.01	3.2	2.18	3.10	3.78	-1.77	0.64	0.68
***ESS*$_B$** (°C)	0.088			0.088			0.088		
solar thermal feedback	f_{ST} W/m²/°C	A_{FT}	***ESS*** °C	f_{ST} W/m²/°C	A_{FT}	***ESS*** °C	f_{ST} W/m²/°C	A_{FT}	***ESS*** °C
	2.05	2.80	0.25	2.12	2.93	0.26	-9.5	0.62	0.06
solar cloud feedback	f_{SC} W/m²/°C	A_{SC}	***ESS*** °C	f_{SC} W/m²/°C	A_{SC}	***ESS*** °C	f_{SC} W/m²/°C	A_{SC}	***ESS*** °C
$c_f = 90$	11.2	3.67	0.33	11.0	3.49	0.31	11.0	3.49	0.31
$c_f = 180$	12.9	6.24	0.55	12.7	5.80	0.51	12.7	5.72	0.51
solar-thermal-cloud feedback		A_{FT^*} A_{SC}	***ESS*** °C		A_{FT^*} A_{SC}	***ESS*** °C		A_{FT^*} A_{SC}	***ESS*** °C
$c_f = 90$		10.2	0.90		10.2	0.90		2.16	0.19
$c_f = 180$		17.4	1.53		17.0	1.48		3.54	0.32

They form the basis for the further calculations of the temperature series and show some smaller deviations from the direct accounting scheme. So, the self-consistency calculation for the solar sensitivity with a thermal amplification for the 2LCM of A_{FT} = 0.62 (slightly smaller than for pure CO_2 feedback) and a solar cloud amplification of A_{SC} = 3.5 gives a small correction with *ESS* = 0.19°C compared to Eq. (9) with 0.2°C. The respective calculation for the CMIP6 data gives 0.90°C compared to the directly deduced value of 0.96°C. Larger deviations have to be expected for the total temperature at increasing feedbacks and solar variability.

4. Simulation of Temperature Records

In this section we present simulations for the temperature trend over the last 140 years, based on the one hand on the CMIP5 and CMIP6 data, and on the other hand on our own calculations. For these simulations we use our advanced 2LCM, which allows to consider the simultaneous influence of CO_2 and solar variations on the climate. The calculations rely on six different *TSI*-time-series and can directly be compared with composed land-sea surface temperature measurements of the Northern Hemisphere (Soon et al. [21]).

4. 1 Simulation with CMIP5/6 Data

Our simulations and their comparison with observed temperature time series cover the period from 1880 up to now (as far as data are available). For the CO_2 increase before 1958 we use palaeo-climate data assuming a level of 280 ppm in 1850, which is continuously increasing up to 315 ppm in 1957, and since 1958 we consult the Mauna Loa measurements (Tans & Keeling [45]).

4.1.1 CMIP5-Simulation

The CO_2 record used for our calculations is displayed in Fig.4a (Green Squares) and can directly be compared with the calculated temperature series T_C based on the 2LCM (Magenta Diamonds) at a constant *TSI* = 1360 W/m^2, but with the CMIP5 data (Table 1). Only a larger *TIC*-feedback of f_{TC} = 0.74 W/m^2/°C was applied to overcome the inconsistency in the specified *ECS* value for the CMIP5 AOGCMs with 3.2°C.

Within the observed interval of CO_2 concentration changes from 280 to 400 ppm (right scale) and with a relatively high feedback amplification of A_{FT} = 3.01 the temperature increases almost linearly with the CO_2-concentration. As this simulation only relies on CO_2 radiative forcing, both graphs proceed parallel to each other with a temperature increase over 135 years of 1.47°C. Also displayed is a logarithmic plot according to (3) with the specifications as listed in Table 1 for CMIP5 (Plum Dots). Over this considered period it develops even faster with 1.7°C, while at 560 ppm both graphs are crossing.

Fig. 4b shows the same simulation only as temperature anomaly ΔT_C (15.2°C subtracted) and as moving average over 20 years (Magenta Diamonds). This graph can be compared with a composed data set (Blue Triangles) consisting on the one hand of rural land data of the Northern Hemisphere (Soon & Connolly [21]) with a weighting of 30% and on the other hand the sea surface data of Kennedy et al. [46] with a weighting of 70%. The temperature increase of 1.2°C, which due to the averaging procedure is now 0.27°C smaller, is still too large, and particularly stronger deviations show up from 1920 till 1970.

So, CO_2 forcing can only explain a monotonic increase of the temperature, and it completely fails to trace any variations over the observed period. Also, it cannot reproduce the observed cloud variations over the 80s and 90s, which would require a much larger thermal cloud feedback, then causing a temperature increase of even 8°C over the Industrial Era.

On the other hand, also considering solar forcing with *SIC*-feedback included and reproducing the observed cloud cover changes, this contributes to additional warming. So, for an increasing

TSI of typically 0.1 - 0.3% over the considered period, together with the CO_2 warming this gives a total warming of 1.6 - 3.2°C. Even using only *TSI* time series with a very flat variation of less than 0.03% (< 0.4 W/m^2 after averaging over the Schwabe cycles, see e.g., Wang et al. [47] and Matthes et al. [48]), this results in a temperature anomaly over the Industrial Era of 1.2 - 1.5°C, which is in clear contradiction to the measured records.

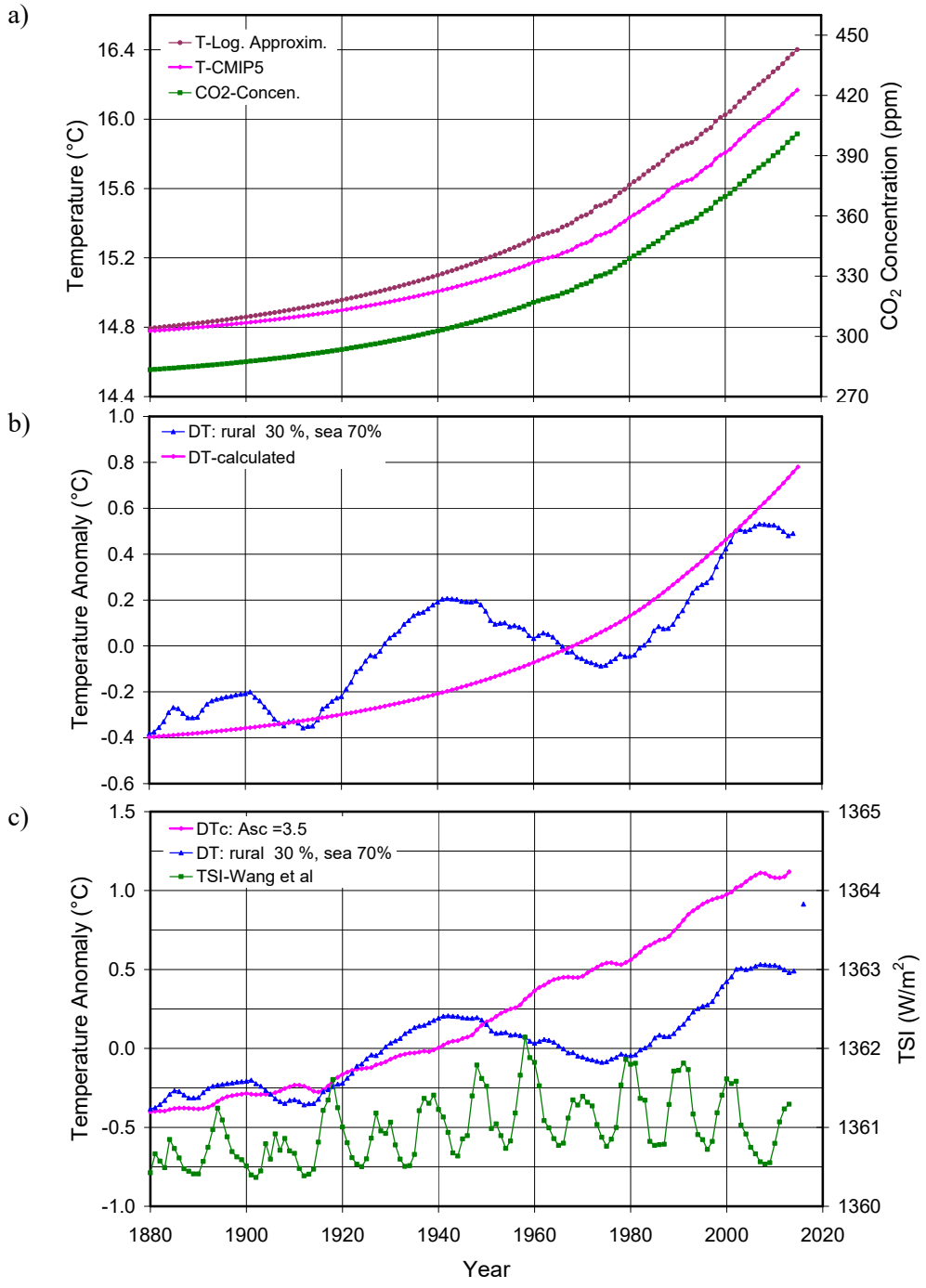

Figure 4: a) Atmospheric CO_2 concentration over time (Green Squares), calculated Earth's temperature with CMIP5 data (Magenta Diamonds) and logarithmic plot (Plum Dots).
b) CMIP5 simulation of temperature anomaly (Magenta Diamonds) compared with composed temperature anomaly (30% rural land, 70% Sea Surface Temperature (SST)) (Blue Triangles).
c) TSI time series of Wang et al. (Green Squares) with calculated temperature anomaly ΔT_C using CMIP5- and TSI-data (Magenta Diamonds) and comparison with composite rural land-sea temperature times series.

Fig. 4c shows the *TSI* series of Wang et al. [47] (Green Squares), which was recommended for the CMIP5 AOGCMs as solar variation over recent years and which is even characterized by a downward trend since the 1970s. The simulated temperature time series based on this *TSI* series with an *ESS* = 0.9°C and otherwise the CMIP5 feedbacks with *ECS* = 3.2°C, is displayed as Magenta Diamonds. To compare it with the composed rural land-sea temperature measurements (Blue Triangles), it is plotted as temperature anomaly (in this case 15.5°C subtracted). It reveals an even larger discrepancy with an increase of more than 1.5°C over the Industrial Era than only considering CO_2 forcing (see Fig. 4b).

4.1.2 CMIP6-Simulation

Fig. 5a shows the respective calculation for the CMIP6 data (Table 1), this for a slightly modified 2LCM with an adapted ECS_B = 1.22°C, a constant *TSI* = 1360 W/m^2 and an *ECS* = 3.78°C (Magenta Diamonds). Over the displayed concentration range, it proceeds again proportional to the CO_2 record (Green Squares) and also to the logarithmic plot (Plum Dots), only with a slightly different slope. Over the considered period of 135 years the temperature increases by 1.81°C (no averaging).

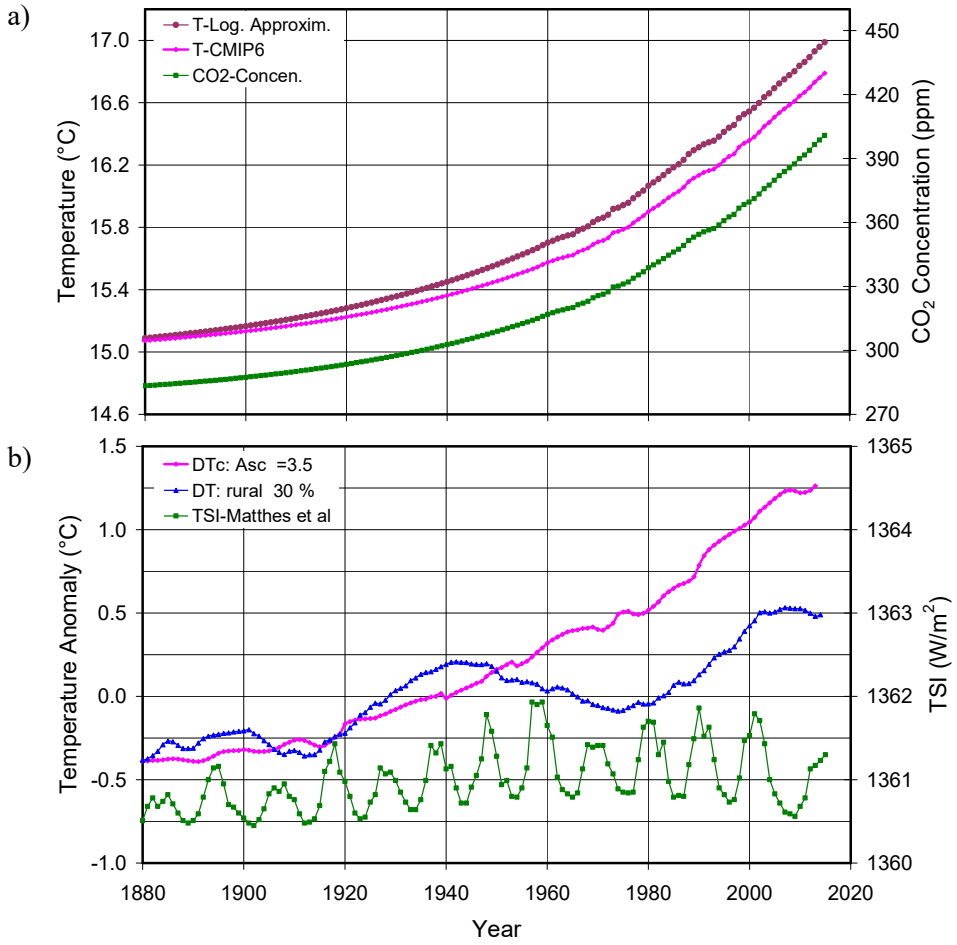

Figure 5: a) Atmospheric CO_2 concentration over time (Green Squares), calculated Earth's temperature T_C with CMIP6 data (Magenta Diamonds) and logarithmic plot (Plum Dots).
b) TSI *time series of Matthes et al. (Green Squares) with calculated temperature anomaly ΔT_C using CMIP6- and TSI-data (Magenta Diamonds) compared with composed temperature anomaly (30% rural land, 70% SST) (Blue Triangles).*

As solar variation for the CMIP6 ESMs is the *TSI* series of Matthes et al. [48] recommended. Fig. 5b shows this series (Green Squares), which significantly differs from the CMIP5 forcing dataset, mainly due to an official reduction of the average *TSI* during solar minimum from

1365.4 W/m^2 to 1361.0 W/m^2 with inevitable implications for understanding the Earth's radiation budget. Besides this significant correction this series is characterized by a very flat progression over time with a variation over the solar cycles (minimum-to-maximum) of 1.5 W/m^2, but for the solar minima of not more than 0.25 W/m^2. For the period from 1983 - 2010, which is important for comparison with the ISCCP observations, it even displays a negative trend like the Wang et al. data. The simulated temperature anomaly based on the Matthes et al. data for an *ESS* = 0.9°C and otherwise the CMIP6 feedbacks is displayed as running average (Magenta Diamonds) and can be compared with the composed rural land-sea temperature measurements (Blue Triangles). With a temperature increase of almost 1.7°C over the Industrial Era it reveals an even larger discrepancy than the CMIP5 simulation. A recent study of Scafetta (2021) [49] comes to a similar conclusion that CMIP6 ESMs are significantly overestimating global warming over the last 40 years.

All this is a strong indication that the observed temperature and cloud changes over the Industrial Era cannot satisfactorily be explained under conditions assumed for the CMIP5 AOGCMs or the CMIP6 ESMs, neither by CO_2 forcing alone nor with additional solar forcing. Although the preceding calculations were performed with our 2LCM, they allow to clearly identify the origin of these deficits. Primarily, we trace them back to the too large total thermal feedbacks used in CMIP5/6 models; and to avoid a still larger dissent to observations, the smallest possible solar influence - and neglecting *SIC*-feedback - is assumed in these models. Instead, IPCC and CMIP5/6 have to consult other effects like negative aerosol feedback to get not too large discrepancies to the observed global warming over the last century.

4. 2 Simulations with Different TSI Time Series Using own Feedback Data

In this subsection we consider simulations, which are only based on our own calculations for the thermal feedbacks and which include solar radiative forcing with *SIC*-feedback. As *TSI* time series we use the records of Matthes et al. [48], Usoskin et al. [50], Muscheler et al. [51], Bard et al. [52, 53] and Hoyt & Schatten [14, 18] to compare the simulations with composed rural land-sea surface temperature time series of different relative weighting.

4.2.1 TSI Time Series of Matthes et al.

The *TSI*-time series of Matthes et al. [48] has already been used for the CMIP6 simulation (Fig. 5b, Green Squares) and is characterized by a very flat progression over time with a variation over the solar cycles (minimum-to-maximum) of 1.5 W/m^2, but for the solar minima of not more than 0.25 W/m^2. This series is again plotted as Green Squares in Fig. 6.

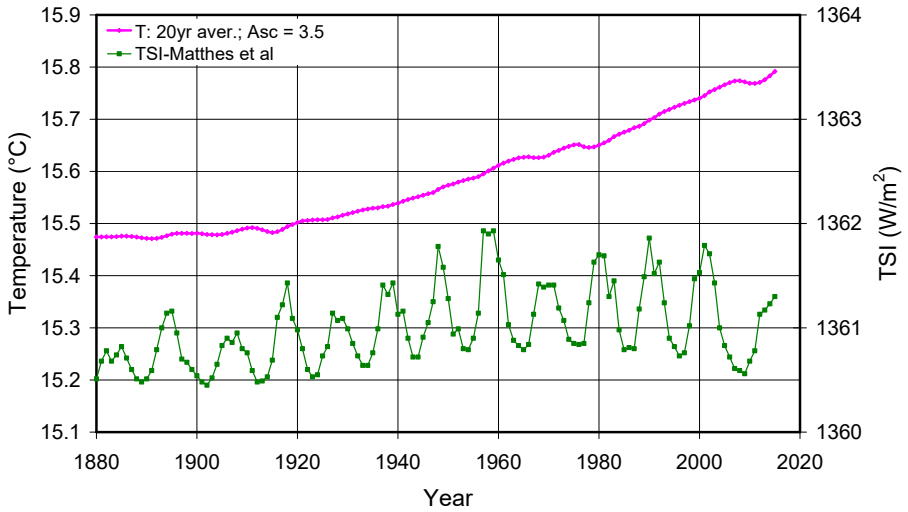

Figure 6: TSI-time-series of Matthes et al. [48] (Green Squares) and simulated Earth's temperature with A_{SC} = 3.5 (Magenta Diamonds).

Apparently for the solar cycles 21 - 23 Matthes et al. and Wang et al. rely on the so called PMOD approach suggested by Fröhlich and Lean [44], who tried to compose two *TSI* satellite datasets within the Active Cavity Radiometer Irradiance Monitor (ACRIM) program, for which data over a gap of 2 yrs were missing. They modified published contributory *TSI* results with the effect of conforming the ACRIM1/ACRIM2 ratio to Earth Radiation Budget Satellite (ERBS) data during the ACRIM gap and matching composite *TSI* to the lower values predicted by solar-proxy models during the activity maximum of solar cycle 21.

This stands in strong contradiction to the ACRIM composite of Willson & Mordvinov [15], who used results originally published by the science teams of contributory experiments and the NIMBUS7/ERB comparisons to relate ACRIM1 and ACRIM2. From their analysis Willson & Mordvinov derived a positive minimum-to-minimum *TSI* trend of 0.05% per decade. They explain the differences to the PMOD approach as an artifact of uncorrected ERBS degradation.

For our further simulations we essentially rely on a positive trend between 0.025% and 0.05% per decade and explain the observed lower cloud cover of 4% within the ISCCP program by this increase (see Eq. (7)). With a $\Delta TSI = 0.025\%$ per decade this requires a solar cloud parameter of $s_f = 180$ and then causes a further amplification of $A_{SC} = 5.7$ and an $ESS = 0.32°C$, for $\Delta TSI = 0.05\%$ per decade s_f is 90, $A_{SC} = 3.5$ and $ESS = 0.19°C$.

The calculated temperature time series based on the Matthes et al. composite is also displayed in Fig. 6 (Magenta Diamonds) and represents a moving average over 20 yr to account for a delayed response of land and oceans to the CO_2 and solar radiative forcings. CO_2 with an increase of almost 120 ppm from 1880 to 2015 and with the thermal feedbacks used for the 2LCM (see Table 1) contributes to a temperature increase of $\Delta T_E^{CO2} = 0.34°C$.

The small solar anomaly of just 0.3 W/m^2 till the mid-century does not donate more than 0.07°C (for $A_{SC} = 3.5$). In such case of a very flat progression, it is close-by to apply also a weaker *TSI* increase over the 80s and 90s for the same cloud change of 4%. Within the observational uncertainties this is a quite realistic scenario. So, with $\Delta TSI = 0.05\%$ over the considered period (2 decades) the cloud parameter rises to $s_f = 180$ and the cloud feedback amplification increases to $A_{SC} = 5.7$ (slightly nonlinear), which then contributes to a solar heating of $\Delta T_E^{Sun} = 0.12°C$.

Altogether this results in a total calculated warming over the Industrial Era of 0.46°C and only represents about half of the observed warming (see Fig. 4b). Opposite to Subsec. 4.1 now this might be explained by too small thermal feedback, but particularly the very monotonic trend over time, dominated by the CO_2 radiative forcing, is a strong indication that some larger native impact is missing, which may be caused by larger solar variations and/or superimposed internal oscillations like the Atlantic-Multi-Decadal-Oscillation (AMO) or Pacific-Decadal-Oscillation (PDO).

4.2.2 TSI Time Series of Usoskin et al.

The time series of Usoskin et al. [50] shows a stronger dip around 1910 before it continuously rises till 1960 by about 2 W/m^2 and then remains at an almost constant level (Fig.7a, Green Squares). With a cloud amplification of $A_{SC} = 3.5$ the temperature change over the displayed period amounts 0.53°C (Magenta Diamonds).

Better agreement between measured temperatures and our simulations can be found, when assuming a higher *SIC*-feedback amplification of $A_{SC} = 5.7$. This is again justified due to the flat *TSI* trend over the 80s and 90s. Fig. 7b shows the direct comparison of the calculated anomaly (Magenta Diamonds) with the land-ocean temperature time series (Blue Triangles).

While the stronger decline in the early 20th century and the subsequent increase can acceptably be reproduced, the simulation fails to explain the deeper dip around 1970.

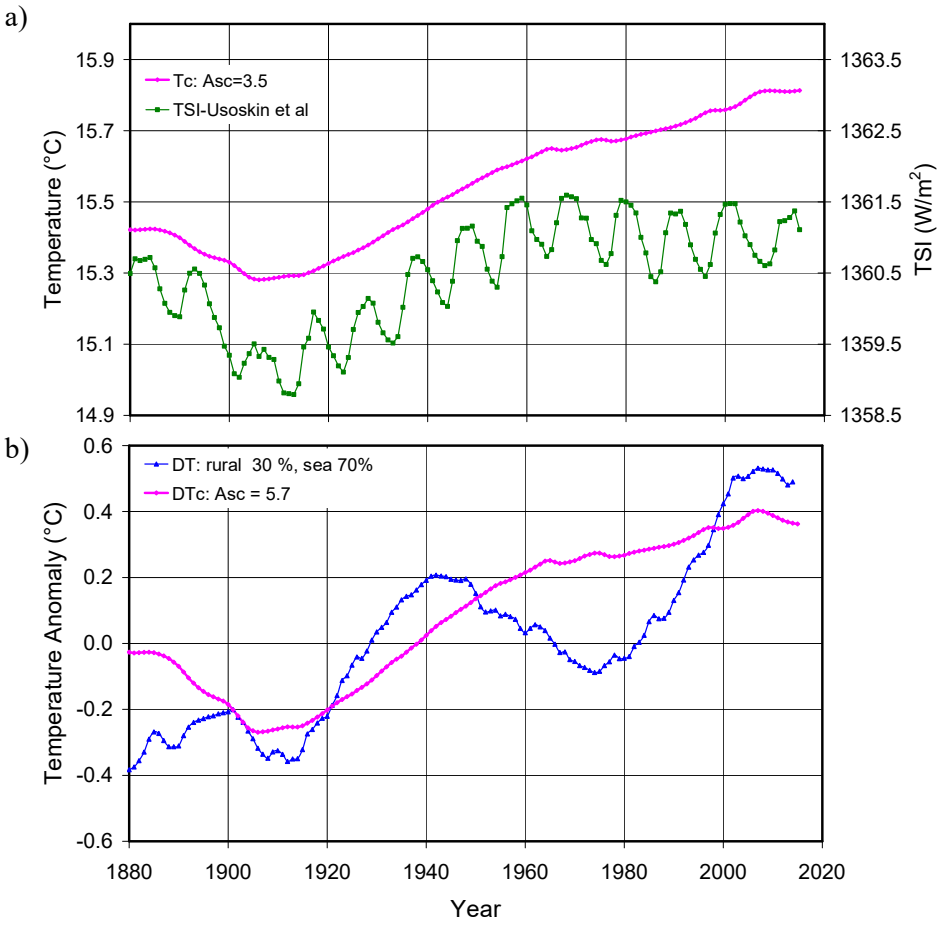

Figure 7: a) TSI-*time-series of Usoskin et al. [50] (Green Squares) and simulated temperature T_C with A_{SC} = 3.5 (Magenta Diamonds). b) Simulated temperature series anomaly ΔT_C applying TSI data of Usoskin et al. for A_{SC} = 5.7 (Magenta Diamonds) compared with composed land-sea temperature anomaly (30% rural, 70% SST) (Blue Triangles).*

4.2.3 TSI Time Series of Muscheler et al.

A *TSI* time series similar to Usoskin et al. has been published by Muscheler et al. [51], which also shows a stronger drop around 1910 and then an almost continuous growth till 2015 altogether of 3 W/m^2 (Fig. 8).

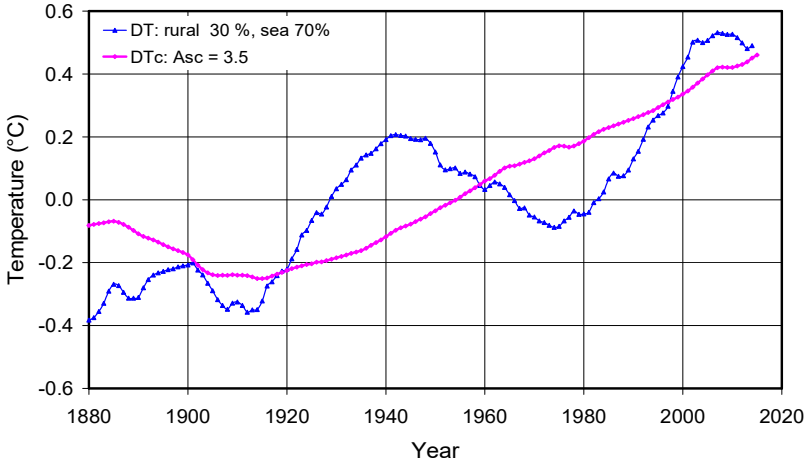

Figure 8: Simulated temperature time series anomaly ΔT_C applying TSI data of Muscheler et al. [51] with A_{SC} = 3.5 (Magenta Diamonds) compared with composed land-sea temperature series (30% rural land, 70% SST) (Blue Triangles).

Additionally, Fig. 8 displays the respective simulation with this *TSI* time series assuming a solar cloud feedback of A_{SC} = 3.5 (Magenta Diamonds).

This simulation reproduces the general temperature increase over the Industrial Era as combination of the CO_2 radiative forcing with an *ECS* = 0.68°C and a solar radiative forcing with *ESS* = 0.19°C (*SIC*-amplification: A_{SC} = 3.5).

But also with this *TSI* time series the stronger temperature variations between the 50s and 80s cannot be explained.

4.2.4 TSI Time Series of Bard et al.

Different to the preceding records the *TSI* time series of Bard et al. [52], updated by Amman et al. [53], shows absolute values, which are about 7 W/m^2 larger than the others (Fig. 9a, Green Squares). This series was derived from cosmogenic isotope records (^{10}Be and ^{14}C) and then adapted to the older recommended *TSI* of 1365.4 W/m^2. As a consequence, also the calculated global temperatures are rising by about 0.5°C. The variations of 1 W/m^2 around the mean *TSI* of 1367 W/m^2 are comparatively small but they confirm quite well the larger decline at the early 20th century, before the intensity is again rising till 1940. For the second half of the century this time series reveals a further wider, pronounced minimum, before the *TSI* rapidly inclines over the 80s and 90s.

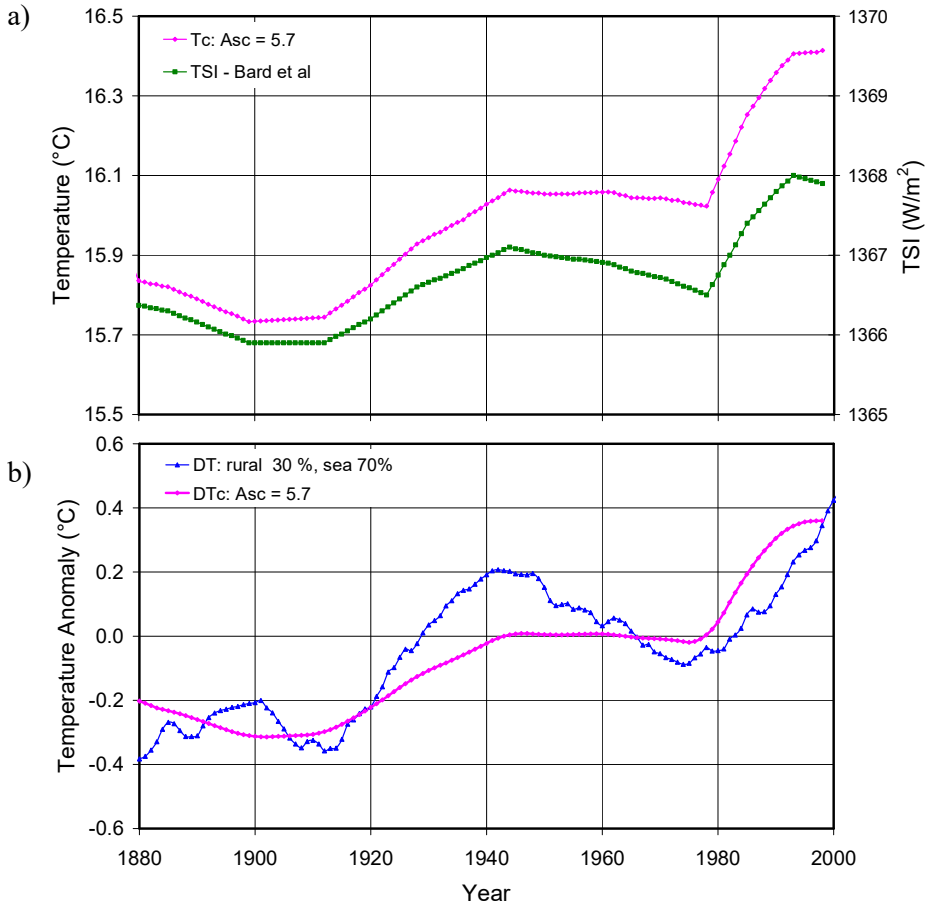

Figure 9: a) TSI time series after Bard et al. [52] (Green Squares) and calculated Earth's temperature T_C assuming a SIC-amplification of A_{SC} = 5.7 (Magenta Diamonds). b) Calculated temperature anomaly ΔT_C (Magenta Diamonds) compared with the composed land ocean temperature time series (30% rural land, 70% SST) (Blue Triangles).

The simulation based on this time series is represented as Magenta Diamonds in Fig. 9a and as temperature anomaly plotted in Fig. 9b, the latter allowing direct comparison with the composed

land-sea temperature series (Blue Triangles). This calculation was performed for a *SIC*-amplification of A_{SC} = 5.7 to compensate for the relatively flat trend of the *TSI* series over the full-time scale.

Although this simulation cannot completely reproduce the distinct modulation of the observed data, this is a clear indication that at least part of these variations could have solar origin.

4.2.5 TSI Time Series of Hoyt & Schatten

Finally, we consider the *TSI* time series of Hoyt & Schatten [14], updated by Scafetta & Willson [18], which similar to the Bard et al. series also shows a reduced solar activity over the 50s till 80s but much more pronounced with a decline of almost 2 W/m^2 (Fig. 10a, Green Squares). This strong solar variability has already extensively been discussed by Soon et al. [21] and shown to be the dominant influence on Northern Hemisphere temperature trends since at least 1881.

Our actual simulations with this *TSI* time series integrated in the 2LCM confirm the strong correlation between the solar variations and observed temperature records over the last century. Fig. 10a displays the non-averaged calculated temperature trend (Plum Dots) to compare this directly with the *TSI* series and to demonstrate how the calculation closely tracks the solar variations. Additionally, Fig. 10a reveals the smoothed data as running average over 20 yr (Magenta Diamonds), clearly exposing the phase shift mainly expected due to the delayed response by the oceans.

Fig. 10b shows the simulated temperature anomaly (Magenta Diamonds) and the composed rural land-ocean temperature series with a weighting of 30% rural land and 70% oceans (Blue Triangles). Similar to the calculation with the other *TSI* series also here we find better agreement with observations, when assuming a larger cloud feedback with an amplification of A_{SC} = 5.7, respectively an equilibrium solar sensitivity of *ESS* = 0.32°C. Apparently this is an indication of a more sensitive cloud response to *TSI* changes than assuming a solar cloud cover parameter of s_f = 90 (A_{SC} = 3.5) and *ESS* = 0.19°C.

A larger deviation is only found for the late 19th and early 20th century. The correlation factor for this calculation with the composed temperature data is r = 0.95. Assuming a composed temperature series of only 10% land and 90% ocean weighting (Fig. 10c, Blue Triangles) and starting the comparison with the calculation (Magenta Diamonds) at 1908, this correlation is almost perfect (r = 0.99), indicating a slightly larger sensitivity of our simulation to the SST-data.

The deviations between 1880 and 1910 can reasonably well be explained by the AMO with its positive phase during this interval and with a dominant oscillation period of 50 to 70 years. This oscillation also shapes the further temperature development over the 20th and beginning 21st century and apparently develops synchronously with the solar variations. So, part of the distinctive temperature modulation may also be assigned to this or additional superimposed native forcings. But also without these impacts solar radiative forcing and its amplification by induced cloud changes can already well explain the observed temperature changes. In any way can the AMO like other observed beats in a more general way be traced back to solar wind and planetary gravitation interactions, reflecting harmonic and sub-harmonic beats of the solar cycles (for a detailed discussion, see Mörner et al., 2020 [54], Subsec. 8.1; for the 60-yrs beats and their origin see also: Scafetta, 2010 [55], 2013 [56]; Solheim 2013 [57]). Therefore, in a wider sense may also these additional forcings be understood as solar and gravitation-controlled drivers, whose strength and periodicity to some part is also mirrored in the *TSI*-variations.

While the CO_2 increase over the Industrial Era alone can only explain a temperature growth of 0.34°C of the total observed incline of about 0.9°C, solar radiative forcing in this case contributes about 60% to global warming. For a CO_2 increase of 82 ppm over the last century the respective contribution is not more than 0.24°C or 30% of the calculated increase of 0.84°C over this period.

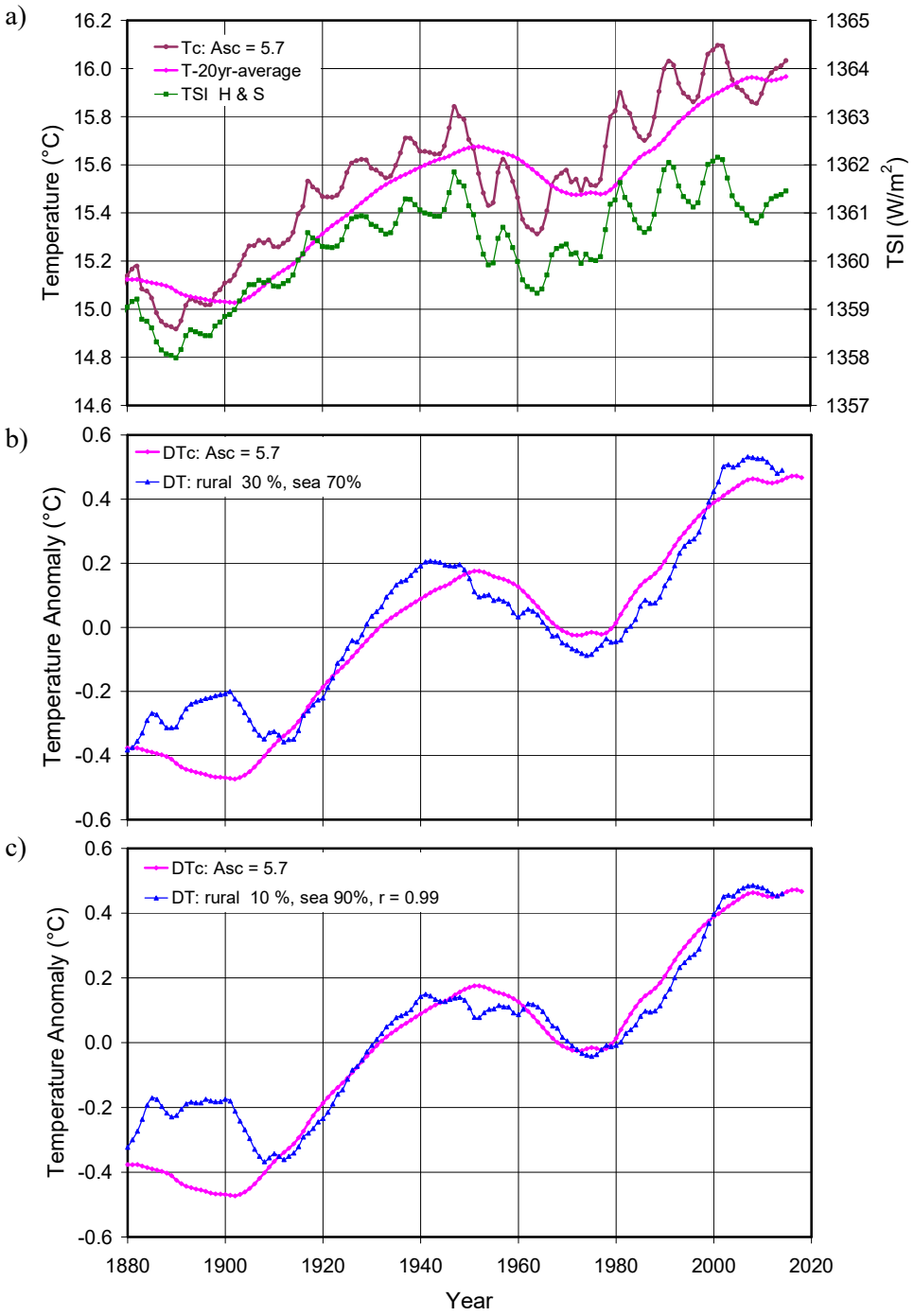

Figure 10: a) TSI time series after Hoyt & Schatten [14] (Green Squares) and calculated temperature trend T_C assuming a SIC-amplification of A_{SC} = 5.7 without averaging (Plum Dots) and with 20 yrs running average (Magenta Diamonds. b) and c) Calculated temperature anomaly ΔT_C (Magenta Diamonds) compared with composed land-sea temperature series b) for 30% rural, 70% SST and c) for 10% rural and 90% SST (Blue Triangles).

5. Conclusion

We have performed detailed studies of CO_2 and solar radiative forcing with their mutual influence on global warming. While the IPCC assumes that most of the temperature trends since the 1950s are due to changes in atmospheric greenhouse gas concentrations (AR5-WG1-SPM-D3

[1] and AR6-WG1-SPM [2]), our own calculations indicate that the temperature increase and its variations over the last 140 years can best be explained by combined CO_2 and solar radiative forcing.

For these investigations we have used an advanced energy-radiation-balance model (Harde [12, 13]), which allows to simulate the global temperature trend under the simultaneous impact of increasing CO_2 concentrations and solar variability. These simulations can directly be compared with observed temperature time series, for which - due to the different response of continents and oceans - we refer to the combined land-ocean-temperature composite of the Northern Hemisphere as derived by Soon & Connolly [21].

Our studies cover simulations under quite contrasting conditions, on the one hand based on the model means of the CMIP5 AOGCMs and CMIP6 ESMs characterized by Equilibrium Climate Sensitivities of *ECS* = 3.2°C (AR5-WG1-Tab.9.5 [1]) and *ECS* = 3.78°C (AR6-WG1-Table 7.SM.5 [2]), on the other hand based on our own calculations of CO_2 radiative forcing with an *ECS* = 0.68°C (Harde [13]). For the solar radiative forcing we considered six different *TSI* time series with significantly different trends (Wang et al. [47]; Matthes et al. [48], Usoskin et al. [50], Muscheler et al. [51], Bard et al. [52, 53] and Hoyt & Schatten [14, 18]), which with respect to their impact on global warming are subject of a further amplification by thermally induced feedbacks as well as solar induced cloud feedback (Harde [12, 13]). Together these amplifications are denoted by the Equilibrium Solar Sensitivity *ESS* (temperature change at ΔTSI = 0.1%) with values varying between 0.19°C and 0.9°C depending on the prevailing feedbacks. The amplification due to cloud changes was derived from observations within the International Satellite Cloud Climatology Project [32] over the 80s and 90s.

From these simulations we see that under CMIP5/6 conditions with large thermal feedback but very flat solar variability (Wang et al. [47] and Matthes et al. [48]) the calculated temperature increase over the Industrial Era is distinctly larger than found from observations. Even CO_2 forcing alone would contribute to a too large warming. Apparently, some inconsistencies between observations and calculations result from the temperature and *TSI* records themselves, which on their part reveal significant differences between each other. Also, the *ECS* and *ESS* values applied in our simulations contain larger uncertainties. But it is also clear that the observed dominant temperature variations over the last century with a broader dip over the 50s to 80s cannot be traced back only to CO_2, which was only monotonically increasing over the considered period and mistakenly is assumed to be only of anthropogenic origin, while a much larger fraction of native origin (about 85%) is obviously embezzled (see Harde [10,11]; Harde & Salby [58]; Salby & Harde [59,60]).

On the other hand, calculations relying on our own CO_2 radiative forcing data with significantly smaller thermal feedback but larger solar variability show excellent agreement with the land-ocean-temperature composite. So a simulation with an *ECS* = 0.68°C, an *ESS* = 0.32°C and based on the *TSI* time series of Hoyt & Schatten [14] reproduces the stronger temperature drop over the 50s till 80s and also the total warming of ~0.9 °C over the considered time interval with a correlation factor of $r = 0.95$.

Our findings confirm the actual studies of Connolly et al. [22] and Stefani [61], who are using a multiple regression analysis to quantify the relative contribution of CO_2 and solar generated global warming. Connolly et al. demonstrate that even up to 98% of global warming over the last 170 years may be explained by solar radiative forcing, depending on the underlying *TSI*-series and temperature time series. Based on a double regression analysis of the temperature data with the geomagnetic aa-index and the logarithm of the CO_2 concentration Stefani derives a correlation around 87% and a transient climate response *TCR* between 0.6°C and 1.6°C for doubling CO_2, which also points to a significant influence of solar variability on the climate.

In this context we emphasize that different to a regression analysis in our studies we independently deduce the absolute CO_2 radiative forcing and solar radiative forcing - the latter only dependent on the assumed *TSI* satellite datasets within the ACRIM-program over the 80s and

90s - which we compare with the composed land-sea surface temperature measurements.

Consideration of additional forcings like AMO or other native oscillations may even improve this agreement (see Fig. 10b and 10c), but as long as their size and origin cannot better be identified, is solar radiative forcing and its amplification by induced cloud changes the most plausible explanation for the observed temperature changes, all the more as also the other forcings are more or less controlled by the solar wind and superposed planetary gravitational impacts (Mörner et al. [54]).

From the preceding calculations we derive a CO_2 affected portion to global warming over the Industrial Era of not more than 0.34°C and over the last century of only 0.24°C, which is 30% of the total warming, while apparently two thirds are caused by the solar impact. As human CO_2 emissions should not have contributed more than 15% to the increase over the Industrial Era, the anthropogenic fraction to global warming is expected to be only 0.05°C.

Funding

This research did not receive any specific grant from funding agencies in the public, commercial, or not-for-profit sectors.

Guest-Editor: Prof. Jan-Erik Solheim; Reviewers were anonymous.

Acknowledgements

The author thanks Dr. Willie Soon and Dr. Ronan Connolly, both Center for Environmental Research and Earth Science, Salem, MA, USA, and Dr. Michael Connolly, independent scientist, Dublin, for encouraging this study and for many stimulating discussions.

Special thanks go also to the guest editor Prof. Jan-Erik Solheim and editor Geir Hasnes for additional suggestions and support of this publication.

References

1. Fifth Assessment Report (AR5), IPCC, 2013: T. F. Stocker, D. Qin, G.-K. Plattner et al., Eds., Climate Change 2013: *The Physical Science Basis*, Cambridge University Press, New York, NY, USA, 2014.
2. Sixth Assessment Report (AR6), IPCC, 2021: V. Masson-Delmotte, P. Zhai, A. Pirani et al.: Climate Change 2021: *The Physical Science Basis. Contribution of Working Group I to the Sixth Assessment Report of the Intergovernmental Panel on Climate Change*, Cambridge University Press. In Press.
3. J. R. Petit, J. Jouzel,D. Raynaud et al., 1999: *Climate and atmospheric history of the past 420,000 years from the Vostok ice core*, Antarctica, Nature, vol. 399, no. 6735, pp. 429–436.
4. E. Monnin, A. Indermühle, A. Dällenbach et al., 2001: *Atmospheric CO_2 concentrations over the last glacial termination*, Science, vol. 291, no. 5501, pp. 112–114.
5. N. Caillon, J. P. Severinghaus, J. Jouzel, J.-M. Barnola, J. Kang, and V. Y. Lipenkov, 2003: *Timing of atmospheric CO_2 and antarctic temperature changes across termination III*, Science, vol. 299, no. 5613, pp. 1728–1731.
6. M. S. Torn and J. Harte, 2006: *Missing feedbacks, asymmetric uncertainties, and the underestimation of future warming*, Geophysical Research Letters, vol. 33, no. 10, Article ID L10703.

7. O. Humlum, K. Stordahl, and J.-E. Solheim, 2013: *The phase relation between atmospheric carbon dioxide and global temperature*, Global and Planetary Change, vol. 100, pp. 51–69.
8. M. L. Salby, 2013: *Relationship between Greenhouse Gases and Global Temperature*, video presentation, April 2013, Hamburg, Germany, https://www.youtube.com/watch?v=2ROwcDKwc0.
9. D. Koutsoyiannis, Z. W. Kundzewicz, 2020: *Atmospheric Temperature and CO_2: Hen-Or-Egg Causality?*, Sci 2020, 2, 72; https://doi.org/10.3390/sci2040083
10. H. Harde, 2017: *Scrutinizing the carbon cycle and CO_2 residence time in the atmosphere*, Global and Planetary Change 152, pp. 19-26, http://dx.doi.org/10.1016/j.gloplacha.2017.02.009.
11. H. Harde, 2019: *What Humans Contribute to Atmospheric CO_2: Comparison of Carbon Cycle Models with Observations*. Earth Sciences, Vol. 8, No. 3, pp. 139-158, https://doi.org/10.11648/j.earth.20190803.13.
12. H. Harde, 2014: *Advanced two-layer climate model for the assessment of global warming by CO_2*, Open Journal of Atmospheric and Climate Change, vol. 1, no. 3, pp. 1–50, http://citeseerx.ist.psu.edu/viewdoc/download?doi=10.1.1.909.4771&rep=rep1&type=pdf.
13. H. Harde, 2017: *Radiation Transfer Calculations and Assessment of Global Warming by CO_2*, International Journal of Atmospheric Sciences, Volume 2017, Article ID 9251034, pp. 1-30, https://www.hindawi.com/journals/ijas/2017/9251034/, https://doi.org/10.1155/2017/9251034.
14. D. V. Hoyt, K. H. Schatten, 1993: *A discussion of plausible solar irradiance variations, 1700-1992*, Journal of Geophysical Research: Space Physics 98 18895–906.
15. R. C. Willson and A. V. Mordvinov, 2003: *Secular total solar irradiance trend during solar cycles 21–23*, Geophysical Research Letters, vol. 30, no. 5, pp. 1–4.
16. A. Shapiro, W. Schmutz, E. Rozanov, M. Schoell, M. Haberreiter, and S. Nyeki, 2011: *A new approach to long-term reconstruction of the solar irradiance leads to large historical solar forcing*, Astronomy & Astrophysics, vol. 529, article 67.
17. S. Ziskin andN. J. Shaviv, 2012: *Quantifying the role of solar radiative forcing over the 20th century*, Advances in Space Research, vol. 50, no. 6, pp. 762–776.
18. N. Scafetta and R. C. Willson, 2014: *ACRIM total solar irradiance satellite composite validation versus TSI proxy models*, Astrophysics and Space Science, vol. 350, no. 2, pp. 421–442, http://dx.doi.org/10.1007/s10509-013-1775-9.
19. I. G. Usoskin, G. Hulot, Y. Gallet et al., 2014: *Evidence for distinct modes of solar activity*, Astronomy & Astrophysics, vol. 562, article L10.
20. X. Zhao and X. Feng, 2014: *Periodicities of solar activity and the surface temperature variation of the Earth and their correlations*, Chinese Science Bulletin, vol. 59, no. 14, pp. 1284–1292.
21. W. Soon, R. Connolly, and M. Connolly, 2015: *Re-evaluating the role of solar variability on Northern Hemisphere temperature trends since the 19th century*, Earth-Science Reviews, vol. 150, pp. 409–452.
22. R. Connolly, W. Soon, M. Connolly, S. Baliunas, J. Berglund, C. J. Butler, R. G. Cionco, A. G. Elias, V. M. Fedorov, H. Harde, G. W. Henry, D. V. Hoyt, O. Humlum, D. R. Legates, S. Lüning, N. Scafetta, J.-E. Solheim, L. Szarka, H. van Loon, V. M. V. Herrera, R. C. Willson, H. Yan and W. Zhang, 2021: *How much has the Sun influenced Northern Hemisphere temperature trends? An ongoing debate*, Research in Astronomy and Astrophysics 2021 Vol. 21 No. 6, 131(68pp), http://www.raa-journal.org/raa/index.php/raa/article/view/4906.

23. H. Harde, 2011: *Was trägt CO_2 wirklich zur Globalen Erwärmung bei?: Spektroskopische Untersuchungen und Modellrechnungen zum Einfluss von H_2O, CO_2, CH_4 und O_3 auf unser Klima*, Books on Demand, Norderstedt, Germany.

24. H. Harde, 2013: *Radiation and heat transfer in the atmosphere: a comprehensive approach on a molecular basis*, International Journal of Atmospheric Sciences, vol. 2013, Article ID 503727, 26 pages, http://dx.doi.org/10.1155/2013/503727.

25. L. S. Rothman, I. E. Gordon, A. Barbe et al., 2008: *The HITRAN 2008 molecular spectroscopic database,* Journal Of Quantitative Spectroscopy and Radiative Transfer, vol. 110, no. 9-10, pp. 533–572, 2008,
New Version (2016): High-Resolution Transmission Molecular Absorption data base, Harvard-Smithsonian Center for Astrophysics: https://www.cfa.harvard.edu/hitran/.

26. K. E. Trenberth, J. T. Fasullo, and J. Kiehl, 2009: *Earth's global energy budget*, Bulletin of the American Meteorological Society, vol. 90, no. 3, pp. 311–323.

27. B. Barkstrom, E. Harrison, G. Smith et al., 1985: *Earth Radiation Budget Experiment (ERBE) archival and April 1985 results*, Bulletin of the American Meteorological Society, vol. 70, pp. 1254–1262.

28. T. D. Bess and G. L. Smith, 1993: *Earth radiation budget: results of outgoing longwave radiation from Nimbus-7, NOAA-9 and ERBS satellites*, Journal of Applied Meteorology, vol. 32, no. 5, pp. 813–824.

29. B. A. Wielicki, B. R. Barkstrom, E. F. Harrison, R. B. Lee III, G. L. Smith, and J. E. Cooper, 1996: *Clouds and the Earth's radiant energy system (CERES): an earth observing system experiment*, Bulletin of the American Meteorological Society, vol. 77, no. 5, pp. 853–868.

30. B. A. Wielicki, B. R. Barkstrom, E. F. Harrison et al., 2006: *CERES radiation budget accuracy overview*, in Proceedings of the 12th Conference on Atmospheric Radiation, vol. 9.1, American Meteorological Society, Madison, Wis, USA.

31. T. Wong, B. A. Wielicki, R. B. Lee III, G. L. Smith, K. A. Bush, and J. K.Willis, 2006: *Reexamination of the observed decadal variability of the earth radiation budget using altitude-corrected ERBE/ERBS nonscanner WFOV data*, Journal of Climate, vol. 19, no. 16, pp. 4028–4048.

32. International Satellite Cloud Climatology Project (ISCCP), http://isccp.giss.nasa.gov/products/onlineData.html.

33. O. Humlum, http://www.climate4you.com/index.htm.

34. G. Myhre, E. J. Highwood, K. P. Shine, and F. Stordal, 1998: *New estimates of radiative forcing due to well mixed greenhouse gases*, Geophysical Research Letters, vol. 25, no. 14, pp. 2715–2718.

35. S. Vey, 2007: *Bestimmung und Analyse des atmosphärischen Wasserdampfgehaltes aus globalen GPS-Beobachtungen einer Dekade mit besonderem Blick auf die Antarktis* [Ph.D. thesis], Technical University Dresden.

36. J.-L. Dufresne and S. Bony, 2008: *An assessment of the primary sources of spread of global warming estimates from coupled atmosphere-ocean models*, Journal of Climate, vol. 21, no. 19, pp. 5135–5144.

37. A. C. Clement, R. Burgman, and J. R. Norris, 2009: *Observational and model evidence for positive low-level cloud feedback*, Science, vol. 325, no. 5939, pp. 460–464.

38. R. S. Lindzen,M.-D. Chou, and A. Y. Hou, 2001: *Does the earth have an adaptive infrared iris?,* Bulletin of the American Meteorological Society, vol. 82, no. 3, pp. 417–432.

39. B. A. Laken and E. Pallé, 2012: *Understanding sudden changes in cloud amount: the Southern Annular Mode and South American weather fluctuations*, Journal of Geophysical Research Atmospheres, vol. 117, no. 13, pp. 1984–2012.

40. H. Cho, C.-H. Ho, and Y.-S. Choi, 2012: *The observed variation in cloud-induced longwave radiation in response to sea surface temperature over the Pacific warm pool from MTSAT-1R imagery*, Geophysical Research Letters, vol. 39, no. 18, Article ID L18802.

41. P. M. Caldwell, Y. Zhang, and S. A. Klein, 2013: *CMIP3 subtropical stratocumulus cloud feedback interpreted through a mixed layer model*, Journal of Climate, vol. 26, no. 5, pp. 1607–1625.

42. F. Vahrenholt, S. Lüning, 2012: *Die Kalte Sonne*, Hoffmann und Campe, Hamburg, Germany.

43. H. Svensmark, 2019: *FORCE MAJEURE - The Sun's Role in Climate Change*, The Global Warming Policy Foundation, ISBN 978-0-9931190-9-5.

44. C. Fröhlich and J. Lean, 1998: *The Sun's total irradiance: cycles and trends in the past two decades and associated climate change uncertainties*, Geophys. Res. Lett., 25, 4377– 4380.

45. P. Tans, NOAA/ESRL and R. Keeling, Scripps Institution of Oceanography (scripp-sco2.ucsd. edu/), 2017, https://www.esrl.noaa.gov/gmd/ccgg/trends/data.html.

46. J. J. Kennedy, N. A. Rayner, C. P. Atkinson and R. E. Killick, 2019: *An Ensemble Data Set of Sea Surface Temperature Change From 1850: The Met Office Hadley Centre HadSST.4.0.0.0 Data Set,* Journal of Geophysical Research: Atmospheres 124, pp. 7719–63.

47. Y.-M. Wang, J. L. Lean, N. R. Sheeley Jr., 2005: *Modelling the Sun's magnetic field and irradiance since 1713*, Astrophys. J. 625, 522–538, http://dx.doi.org/10.1085/429689.

48. K. Matthes, B. Funke, M. E. Andersson et al., 2017: *Solar forcing for CMIP6*, Geosci. Model Dev., 10, 2247, https://www.geosci-model-dev.net/10/2247/2017/gmd-10-2247-2017.pdf.

49. N. Scafetta, 2021: *Testing the CMIP6 GCM Simulations versus Surface Temperature Records from 1980–1990 to 2011–2021: High ECS Is Not Supported*, Climate 9, p. 161, https://doi.org/10.3390/cli9110161

50. I. G. Usoskin, Y. Gallet, F. Lopes, G. A. Kovaltsov & G. Hulot, 2016: *Solar activity during the Holocene: the Hallstatt cycle and its consequence for grand minima and maxima*, Astronomy & Astrophysics, V 587, A150, 10 pp, https://ui.adsabs.harvard.edu/abs/2016A%26A...587A.150U/abstract

51. R. Muscheler, F. Adolphi, K. Herbst & A. Nilsson, 2016: *The Revised Sunspot Record in Comparison to Cosmogenic Radionuclide-Based Solar Activity Reconstructions,* Sol. Phys., 291, 3025, https://ui.adsabs.harvard.edu/abs/2016SoPh..291.3025M/abstract

52. E. Bard, G. Raisbeck, F. Yiou, J. Jouzel, 2000: *Solar irradiance during the last 1200 years based on cosmogenic nuclides*, Tellus 52B, 985–992, http://dx.doi.org/10.3402/tellusb.v52i3.17080.

53. C. M. Ammann, F. Joos, D. S. Schimel, B. L. Otto-Bliesner, R. A. Tomas, 2007: *Solar influence on climate during the past millennium: results from transient simulations with the NCAR Climate System Model,* Proc. Natl. Acad. Sci. 104, 3713–3718, http://dx.doi.org/10.1073/pnas.0605064103.

54. N.-A. Mörner, J.-E. Solheim, O. Humlum, S. Falk-Petersen, 2020: *Changes in Barents Sea Ice Edge Positions in the Last 440 Years: A Review of Possible Driving Forces*, Intern. Journal of Astronomy and Astrophysics, 2020, 10, 97-164, https://www.scirp.org/journal/ijaa.

55. N. Scafetta, 2010: *Empirical Evidence for a Celestial Origin of the Climate Oscillations and its Implications*, Journal of Atmospheric and Solar-Terrestrial Physics , 72, pp. 951-970, https://doi.org/10.1016/j.jastp.2010.04.015.

56. N. Scafetta, 2013: *Solar and Planetary Oscillation Control on Climate Change: Hind-Cast, Forecast and a Comparison with CMIP5 GCMS*, Energy & Environment, 24, pp. 455-496, https://doi.org/10.1260/0958-305X.24.3-4.455.

57. J.-E. Solheim, 2013: *Signals from the Planets, via the Sun to the Earth*, Pattern Recognition in Physics , 1, pp. 177-184, https://doi.org/10.5194/prp-1-177-2013.

58. H. Harde, M. L. Salby, 2021: *What Controls the Atmospheric CO_2 Level?*, Science of Climate Change and Philosophy Vol. 1, No.1, pp. 54 - 69, https://doi.org/10.53234/scc202106/22.

59. M. L. Salby, H. Harde, 2021: *Control of Atmospheric CO_2 - Part I: Relation of Carbon 14 to Removal of CO_2*, Science of Climate Change and Philosophy Vol. 1, No.2, pp. 177-195, https://doi.org/10.53234/scc202112/30.

60. M. L. Salby, H. Harde, 2021: *Control of Atmospheric CO_2 - Part II: Influence of Tropical Warming*, Science of Climate Change and Philosophy Vol. 1, No.2, pp. 196-212, https://doi.org/10.53234/scc202112/12.

61. F. Stefani, 2021: *Multiple regression analysis of anthropogenic and heliogenic climate drivers, and some cautious forecasts*, Climate 9(11), p. 163, https://doi.org/10.3390/cli9110163.

Annex: Acronyms

Abbreviation	**meaning**
2LCM	Two-Layer Climate Model
ACRIM	Active Cavity Radiometer Irradiance Monitor
A_{FT}, A_{SC}	thermal feedback amplification, solar induced cloud amplification
AGW	Anthropogenic Global Warming
AMO, PDO	Atlantic-Multi-Decadal-Oscillation, Pacific-Decadal-Oscillation
a_{LW}	long wave absorptivity (of CO_2, WV, CH_4 and O_3)
a_{SW}	short wave absorptivity (of CO_2, WV, CH_4 and O_3)
AR5	Fifth Assessment Report of the IPCC (2013)
AR6	Sixth Assessment Report of he IPCC (2021)
AOGCMs	atmosphere-ocean general circulation models
C, C_R	CO2 concentration, reference concentration 350 ppm
C_C, C_{CR}	cloud cover, reference cloud cover 66%
CERES	Clouds and the Earth's Radiant Energy System
CMIP5, CMIP6	Coupled Model Intercomparison Project Phase 5, Phase 6
ΔF_{CO2}, ΔF_{Sun}	CO2 and solar radiative forcing
ΔT_C	calculated temperature anomaly
ΔTSI	total solar irradiance variability
EASy	Earth-Atmosphere-System
ECS	equilibrium climate sensitivity

EMICs	Earth System Models of Intermediate Complexity
ERBE	Earth Radiation Budget Experiment
ERBS	Earth Radiation Budget Satellite
ESMs	Earth-system models
ESS	equilibrium solar sensitivity
α_P	Planck feedback
f_A	downward directed fraction of atmospheric radiation
f_{WV}, f_{LR}, f_{SA}, f_{CO}, f_{EV}, f_{TC}	feedbacks: WV, lapse rate, surface albedo, convection, evaporation, cloud
f_{TG}, f_{SC}, f_{ST}	total thermal feedbacks, solar induced cloud, solar induced thermal feedb.
GH-gases	green house gases
GPS	global positioning satellite
HadCRUT	Hadley Centre and Climate Research Unit
IPCC	Intergovernmental Panel of Climate Change
ISCCP	International Satellite Cloud Climatology Project
λ_P	Planck sensitivity - climate sensitivity parameter
λ_{Sun}	solar sensitivity parameter
LBL-RT calculations	line-by line radiation transfer calculations
lw radiation	long wave radiation
P_A, P_E	radiated power of atmosphere and of Earth's surface
ppm, ppmv	parts per million by volume
r	correlation factor
RF	radiative forcing
s_f	solar induced cloud cover parameter
SIC-feedback	solar induced cloud feedback
S_R	reference solar constant
SST	sea surface temperature
sw radiation	short wave radiation
T_A, $T_{E,}$	atmospheric temperature (lower troposphere), Earth (surface) temperature
T_C, T_{Cl}	calculated temperature series, cloud temperature,
T_R	reference temperature (15.5 °C)
TCR	Transient Climate Response
TFK-scheme	energy and radiation budget scheme after Trenberth et al. [26]
TIC-feedback	thermally induced cloud feedback
TSI	total solar irradiance
WV	water vapor